mmHg in order to estimate the static characteristics of the CSP-BNA transduction.

We recorded CSP, BNA and AP at a sampling rate of 200 Hz by using a 12-bit analog-to-digital converter. The data were stored on the hard disk of a dedicated laboratory computer system for later analysis.

Data analysis. In the random input protocol, we estimated the transfer function, $H(f)$, from CSP input to BNA output according to previous studies [1–4, 8, 10–11, 13]. We normalized the transfer function so that the average transfer gain value below 0.02 Hz became unity and expressed BNA in arbitrary units for dynamic analysis (AU_{dyn}). We also calculated the coherence function, $Coh(f)$, between CSP and BNA [1–4, 8, 10–11, 13]. A unity coherence value indicates perfect linear dependence whereas zero coherence value indicates total independence between CSP and BNA.

In the stepwise input protocol, we calculated the steady-state BNA values by averaging the data during the last 10 s of each CSP level. We then scaled these values so that their minimum and maximum BNA values became 0 and 100 arbitrary units (AU_{stat}), respectively, for static analysis. We performed a regression analysis for the four-parameter logistic function using Eq. 1 [14].

$$y = \frac{P_1}{1+\exp[P_2(x-P_3)]} + P_4 \qquad (1)$$

where P_1 is the response range (i.e., the difference between the maximum and minimum values of y), P_2 is the slope coefficient, P_3 is the midpoint on the input axis, and P_4 is the minimum value of y. The fitting error (err%) for the logistic function was evaluated by using Eq. 2.

$$err\% = \frac{\sum_{k=1}^{N}[u(k)-y(k)]^2}{\sum_{k=1}^{N}[u(k)-\bar{u}]^2} \times 100 \qquad (2)$$

where u(k) and y(k) indicate the measured and predicted BNA values at each CSP level. N indicates the number of data points analyzed, and $\bar{u}$ represents the average value of u(k) when k spans from 1 to N.

RESULTS

The dynamic characteristics of the pressure transduction from CSP to actual pressure imposed on the carotid sinus area are depicted in Fig. 1A. The gain plot (top panel) indicates the ratio of actual pressure to CSP in the frequency domain. The controlled CSP faithfully reflected the actual pressure up to 3 Hz. The ratio was greatly dispersed above 3 Hz. The phase plot (middle panel) indicates that the phase delay was negligible up to 1 Hz. The phase delay at 3 Hz was approximately 0.33 radians. The coherence plot (bottom panel) indicates that the coherence was unity up to 3 Hz and decreased slightly above 3 Hz.

Figure 1B shows a typical time series of CSP and BNA obtained from the random input protocol. CSP was changed according to a binary white noise sequence. BNA varied in response to the CSP input. When CSP was increased, BNA was increased, and vice versa.

Figure 1C illustrates the transfer function from CSP to BNA averaged from all animals. The gain plot (top), phase plot (middle) and coherence plot (bottom) are presented. In each plot the thick line indicates the mean value, and the thin lines indicate the mean ± SEM values. In the gain plot, the gain value at the lowest frequency was normalized to unity. The gain increased with increasing frequency from 0.01 to 0.3 Hz and showed a relatively constant value of approximately 1.7 up to 3 Hz. In the phase plot, the phase value led slightly in the frequency range from 0.01 to 0.2 Hz and close to zero radians from 0.2 to 1 Hz. Although the phase delayed above 1 Hz, the delay is most likely attributable to the phase delay between CSP and actual pressure shown in Fig. 1A. In the coherence plot, the coherence was approximately 0.6 at the lowest frequency and increased to 0.8 in the frequency range of 0.1 to 3 Hz.

Figure 2A depicts the typical time series of CSP and BNA obtained from the stepwise input protocol. The CSP and BNA data were resampled at 2 Hz for these panels. An increase in CSP increased BNA in the CSP range of 40 to 160 mmHg. When the BNA response to stepwise input was obvious, it was greater at the onset of pressure change and then decayed to the steady-state value. The steady-state BNA value was not necessarily greater at 40 mmHg than at 20 mmHg across the animals. The steady-state BNA value was not necessarily greater at 180 mmHg than at 160 mmHg.

Figure 2B illustrates the static input-output relationship between CSP and BNA averaged from all animals. The closed circles and error bars represent mean and mean ± SEM values of BNA at each CSP level, respectively. The solid curve indicates the logistic function constructed from the averaged parameters shown in Table 1.

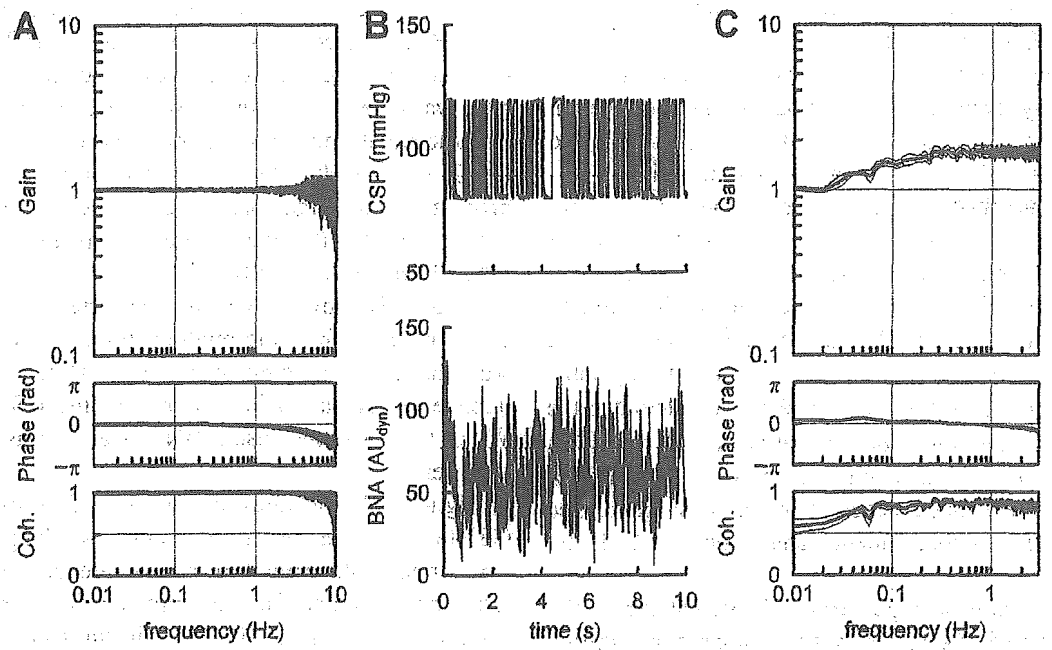

Fig. 1. A: The transfer function from controlled carotid sinus pressure (CSP) to actual pressure imposed on the carotid sinus area. The gain plot represents the ratio of actual pressure to CSP in the frequency domain. The phase plot represents the phase difference between CSP and actual pressure. The coherence (Coh.) shows the extent of linearity between CSP and actual pressure. Based on the transfer function from CSP to actual pressure, we employed the transfer function data up to 3 Hz in the analysis of CSP-nerve activity transduction. The phase difference between CSP and actual pressure in the frequency range between 1 and 3 Hz was taken into account in the interpretation of the CSP-nerve activity transduction. **B: Representative time series of CSP and afferent baroreceptor nerve activity (BNA) during the random input protocol.** CSP was changed according to a binary white noise signal with a switching interval of 50 ms. AU_{dyn}: arbitrary units for dynamic analysis. **C: Transfer function from CSP to BNA averaged from all animals.** The gain plot, phase plot, and coherence are shown. The transfer gain increased with increasing frequency from 0.01 to 0.3 Hz and showed a relatively constant value of approximately 1.7 up to 3 Hz. In all panels, thick and thin lines represent mean and mean ± SEM values.

Table 1 summarizes the parameters of the logistic function fitted to the steady-state CSP-BNA relationship obtained from the stepwise input protocol. The fitting error to the logistic function was less than 1% relative to the total variation in steady-state BNA values.

DISCUSSION

Dynamic characteristics of the carotid sinus baroreceptor transduction. Because of technical difficulty with the in situ preparation, we could not measure actual pressure imposed on the carotid sinus area and record BNA simultaneously. Therefore we measured controlled CSP and actual pressure imposed on the carotid sinus area simultaneously. As shown in Fig. 1A, the controlled CSP faithfully reflected the actual pressure up to 3 Hz. Above this frequency the ratio of actual pressure to CSP became greatly dispersed among animals. Because the compliance of the isolated area would depend on the vascular configuration and inevitably differ among animals, the pressure transduction in the frequencies above 3 Hz may reveal significant inter-individual differences. Actually, the insertion of the catheter-tip micromanometer itself might have affected the compliance of the isolated area to some degree. The phase delay reached approximately 0.33 radians at 3 Hz, which corresponds to 0.018 s of pure dead time. Although this value was not negligible, we employed the transfer function data up to 3 Hz in the analysis of the CSP-BNA relationship because the inter-individual differences in the phase delay were

Table 1. Parameters of the logistic function fitted to the steady-state CSP-BNA relationship.

Response range, P_1, AU_{stat}	98.1 ± 2.4
Slope coefficient, P_2, $mmHg^{-1}$	−0.072 ± 0.010
Midpoint pressure, P_3, mmHg	89.9 ± 3.4
Minimum value, P_4, AU_{stat}	0.05 ± 1.98
err%	0.9 ± 0.5

Data are means±SEM.

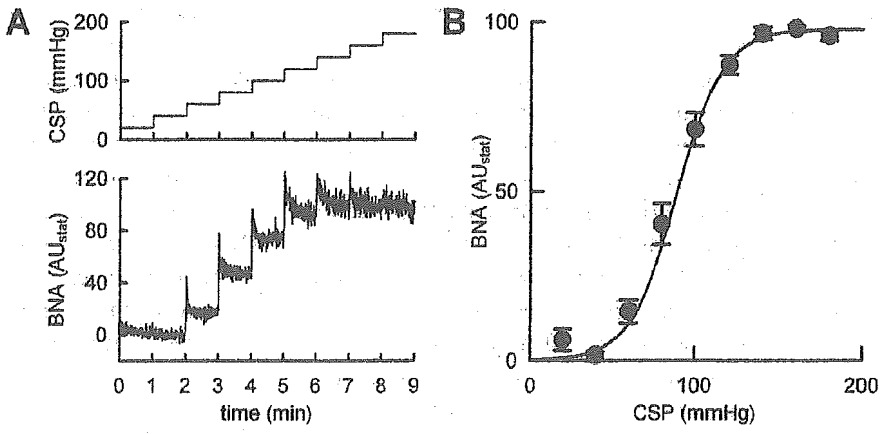

Fig. 2. A: Representative time series of carotid sinus pressure (CSP) and afferent baroreceptor nerve activity (BNA) during the stepwise input protocol. CSP and BNA were resampled at 2 Hz for the panels. CSP was increased from 20 to 180 mmHg every minute with a pressure step of 20 mmHg. **B: The CSP-BNA relationship averaged from all animals.** The CSP-BNA relationship revealed sigmoidal nonlinearity. The closed circles represent mean values, and the error bars indicate mean ± SEM values at each CSP. The solid curve indicates the logistic function derived from averaged parameters shown in Table 1. AU_{stat}: arbitrary units for static analysis.

very small up to 3 Hz. The phase delay between CSP and actual pressure should be taken into account in the interpretation of phase data of the transfer function from CSP to BNA shown in Fig. 1C. The phase delay between CSP and BNA noted in the frequency range above 1 Hz would be chiefly attributable to the phase delay between CSP and the actual pressure imposed on the carotid sinus area.

Derivative characteristics of the baroreflex neural arc contribute to the optimization of the AP regulation by the carotid sinus baroreflex [1]. Although Franz *et al.* [6] reported dynamic characteristics of single baroreceptor fiber activity in the rabbit carotid sinus in the frequency range from 0.078 to 2.5 Hz by using sinusoidal inputs, the derivative characteristics were obscure in that frequency range. As shown in Fig. 1C, dynamic gain from CSP to BNA augmented to approximately 1.7 with increasing frequency from 0.01 to 0.5 Hz, indicating the existence of the derivative characteristics. When the transfer function from CSP input to efferent SNA was identified in our previous study [15], dynamic gain increased to 3.8-fold for cardiac SNA and to 2.3-fold for renal SNA, with increasing frequency from 0.01 to 0.5 Hz (see Fig. 3 in Ref. 15). Thus approximately 40% (for cardiac) and 64% (for renal) of the derivative characteristic may be explained by the dynamic characteristics of the CSP-BNA transduction.

High-cut characteristics of the baroreflex neural arc attenuate high-frequency components in the input pressure and preserve the baroreflex gain against pulsatile pressure [4]. As shown in Fig. 1C, the dynamic gain of the transfer function from CSP to BNA was relatively constant in the frequency range from 0.3 to 3 Hz and showed no high-cut characteristics. Therefore the high-cut characteristics of the baroreflex neural arc are primarily attributable to the central processing from BNA to efferent SNA. In other words, the dynamic characteristics from BNA to efferent SNA should reveal high-cut characteristics with a corner frequency of approximately 0.8 Hz. The mechanism for the putative high-cut characteristics in the central processing remains unclear. The frequency-dependent depression of the signal transduction in the nucleus tractus solitarii (NTS) neurons [16] may be related to the upper frequency limit of central processing. However, the frequency-dependent depression refers to the phenomenon related to the stimulation frequency itself, whereas the high-cut characteristics refer to the attenuation of the system response related to the modulation frequency of the input. Further information is required to reconcile the putative high-cut characteristics and the frequency-dependent depression in the baroreflex central pathway.

The dynamic characteristics of the carotid sinus baroreceptor transduction were generally similar to those of the baroreceptor transduction of the aortic depressor nerve in rabbits [11]. However, a slight difference can be noted as follows. The gain increase from 0.01 to 0.1 Hz was approximately 1.7-fold (4.6 dB/decade) for the carotid sinus baroreceptors (Fig. 1C), whereas it was approximately 2-fold (6.0 dB/decade) for the aortic baroreceptors (see Fig. 5 in Ref. 11). In the rat aortic baroreceptor preparation, Brown *et al.* [5] demonstrated that myelinated fibers showed peaking in the frequency response, whereas unmyelinated fibers did not. The myelinated and unmyelinated fiber composition would affect the dynamic characteristics of multifiber BNA. Brown *et al.* [5] also demonstrated that the peaking of myelinated fiber response reached approximately 4 dB/decade in normotensive rats and approximately 6 dB/decade in spontaneously hyperten-

sive rats. Therefore the difference between the carotid sinus and aortic baroreceptor transductions, though it seems subtle, may reflect the difference in the myelinated and unmyelinated fiber composition and/or the difference in the prevailing pressure between the carotid sinus and aortic baroreceptors.

Static characteristics of the carotid sinus baroreceptor transduction. The static characteristics of the CSP-BNA transduction showed sigmoidal nonlinearity (Fig. 2B). BNA increased with CSP in the pressure range from 40 to 160 mmHg. In the single fiber preparation of the rabbit carotid sinus baroreceptors, the stimulus-response curve is fairly linear in each fiber between threshold pressure and saturation pressure [6]. However, the threshold pressure and the slope of the linear range vary considerably among fibers. Such variations in the static characteristics of single baroreceptor fiber activities are lumped together, possibly forming the sigmoidal relationship between CSP and multifiber BNA. The slope coefficient of the CSP-BNA relationship (Table 1) was smaller than the slope coefficient of the CSP-SNA relationship (0.10–0.12) determined in our previous studies [15, 17, 18]. In other words, the operating range of the system, which is inversely related to the slope coefficient [14], was wider for the CSP-BNA relationship than for the CSP-SNA relationship. The finding is consistent with our speculation, which is based on input-size and operating-point dependence of the baroreflex neural arc transfer function, that the static CSP-BNA relationship alone does not determine the overall nonlinearity of the neural arc characteristics [2, 3].

The midpoint pressure of the CSP-BNA relationship was approximately 90 mmHg, which is lower than the midpoint pressure of the CSP-SNA relationship (100–110 mmHg) determined in our previous studies [15, 17, 18]. The possibility cannot be ruled out, however, that the extensive surgical operation necessary for the BNA recording had altered the mechanical properties of the carotid sinus area differently from the preparation for the carotid sinus isolation alone. Although we had intended to simultaneously record afferent BNA and efferent SNA, the SNA and AP did not respond to the CSP input in the present experimental settings. A large portion of the baroreceptor afferent fibers may have been damaged because of fragility during the preparation. The difficulty results because we could not know, based on the magnitude of BNA, what percent of the nerve fibers were really kept intact. Further efforts are required to directly demonstrate the difference in the static input-output characteristics between the CSP-BNA relationship and the CSP-SNA relationship.

In conclusion, although a slight difference was noted, the dynamic characteristics of the carotid sinus baroreceptor transduction were similar to those of the aortic baroreceptor transduction in rabbits. The CSP-BNA transduction partly explained the derivative characteristics, but not the high-cut characteristics found in the neural arc transfer function from CSP to efferent SNA. The present results suggest the importance of the central processing from BNA to efferent SNA to account for the overall dynamic characteristics of the baroreflex neural arc.

This study was supported by the Health and Labour Sciences Research Grant for Research on Advanced Medical Technology from the Ministry of Health Labour and Welfare of Japan (H14-Nano-002), and by the Program for Promotion of Fundamental Studies in Health Science of the Pharmaceuticals and Medical Devices Agency of Japan.

REFERENCES

1. Ikeda Y, Kawada T, Sugimachi M, Kawaguchi O, Shishido T, Sato T, Miyano H, Matsuura W, Alexander J Jr, and Sunagawa K: Neural arc of baroreflex optimizes dynamic pressure regulation in achieving both stability and quickness. Am J Physiol Heart Circ Physiol 271: H882–H890, 1996
2. Kawada T, Uemura K, Kashihara K, Kamiya A, Sugimachi M, and Sunagawa K: A derivative-sigmoidal model reproduces operating point-dependent baroreflex neural arc transfer characteristics. Am J Physiol Heart Circ Physiol 286: H2272–H2279, 2004
3. Kawada T, Yanagiya Y, Uemura K, Miyamoto T, Zheng C, Li M, Sugimachi M, and Sunagawa K: Input-size dependence of the baroreflex neural arc transfer characteristics. Am J Physiol Heart Circ Physiol 284: H404–H415, 2003
4. Kawada T, Zheng C, Yanagiya Y, Uemura K, Miyamoto T, Inagaki M, Shishido T, Sugimachi M, and Sunagawa K: High-cut characteristics of the baroreflex neural arc preserve baroreflex gain against pulsatile pressure. Am J Physiol Heart Circ Physiol 282: H1149–H1156, 2002
5. Brown AM, Saum W, and Yasui S: Baroreceptor dynamics and their relationship to afferent fiber type and hypertension. Circ Res 42: 694–702, 1978
6. Franz GN, Sher AM, and Ito CS: Small signal characteristics of carotid sinus baroreceptors of rabbits. J Appl Physiol 30: 527–535, 1971
7. Spickler JW and Kezdi P: Dynamic response characteristics of carotid sinus baroreceptors. Am J Physiol 212: 472–476, 1967
8. Marmarelis PZ and Marmarelis VZ: Analysis of Physiological Systems, Plenum, New York, pp 131–221, 1978
9. Kawada T, Fujiki N, and Hosomi H: Systems analysis of the carotid sinus baroreflex system using a sum-of-sinusoidal input. Jpn J Physiol 42: 15–34, 1992
10. Sugimachi M, Imaizumi T, Sunagawa K, Hirooka Y, Todaka K, Takeshita A, and Nakamura M: A new method

to identify dynamic transduction properties of aortic baroreceptors. Am J Physiol Heart Circ Physiol 258: H887–H895, 1990
11. Sato T, Kawada T, Shishido T, Miyano H, Inagaki M, Miyashita H, Sugimachi M, Knuepfer MM, and Sunagawa K: Dynamic transduction properties of in situ baroreceptors of rabbits aortic depressor nerve. Am J Physiol Heart Circ Physiol 274: H358–H365, 1998
12. Pelletier CL, Clement DL, and Shepherd JT: Comparison of afferent activity of canine aortic and sinus nerves. Circ Res 31: 557–568, 1972
13. Bendat J and Piersol A: Random Data 3rd Ed. John Wiley & Sons, New York, pp 189–271, 2000
14. Kent BB, Drane JW, Blumenstein B, and Manning JW: A mathematical model to assess changes in the baroreceptor reflex. Cardiology 57: 295–310, 1972
15. Kawada T, Shishido T, Inagaki M, Tatewaki T, Zheng C, Yanagiya Y, Sugimachi M, and Sunagawa K: Differential dynamic baroreflex regulation of cardiac and renal sympathetic nerve activities. Am J Physiol Heart Circ Physiol 280: H1581–H1590, 2001
16. Liu Z, Chen C, and Bonham AC: Frequency limits on aortic baroreceptor input to nucleus tractus solitarii. Am J Physiol Heart Circ Physiol 278: H577–H585, 2000
17. Kawada T, Uemura K, Kashihara K, Jin Y, Li M, Zheng C, Sugimachi M, and Sunagawa K: Uniformity in dynamic baroreflex regulation of left and right cardiac sympathetic nerve activities. Am J Physiol Regul Integr Comp Physiol 284: R1506–R1512, 2003
18. Yamamoto K, Kawada T, Kamiya A, Takaki H, Miyamoto T, Sugimachi M, and Sunagawa K: Muscle mechanoreflex induces the pressor response by resetting the arterial baroreflex neural arc. Am J Physiol Heart Circ Physiol 286: H1382–H1388, 2004

Am J Physiol Heart Circ Physiol 289: H2641–H2648, 2005.
First published July 29, 2005; doi:10.1152/ajpheart.00642.2005.

Dynamic and static baroreflex control of muscle sympathetic nerve activity (SNA) parallels that of renal and cardiac SNA during physiological change in pressure

Atsunori Kamiya,[1] Toru Kawada,[1] Kenta Yamamoto,[1] Daisaku Michikami,[1] Hideto Ariumi,[1] Tadayoshi Miyamoto,[1] Shuji Shimizu,[1] Kazunori Uemura,[1] Takeshi Aiba,[1] Kenji Sunagawa,[2] and Masaru Sugimachi[1]

[1]*Department of Cardiovascular Dynamics, National Cardiovascular Center Research Institute, Osaka; and*

[2]*Department of Cardiovascular Medicine, Kyusyu University Graduate School of Medical Sciences, Fukuoka, Japan*

Submitted 14 June 2005; accepted in final form 26 July 2005

Kamiya, Atsunori, Toru Kawada, Kenta Yamamoto, Daisaku Michikami, Hideto Ariumi, Tadayoshi Miyamoto, Shuji Shimizu, Kazunori Uemura, Takeshi Aiba, Kenji Sunagawa, and Masaru Sugimachi. Dynamic and static baroreflex control of muscle sympathetic nerve activity (SNA) parallels that of renal and cardiac SNA during physiological change in pressure. *Am J Physiol Heart Circ Physiol* 289: H2641–H2648, 2005. First published July 29, 2005; doi:10.1152/ajpheart.00642.2005.—Despite accumulated knowledge on human baroreflex control of muscle sympathetic nerve activity (SNA), whether baroreflex control of muscle SNA parallels that of other SNAs, in particular renal and cardiac SNAs, remains unclear. Using urethane and α-chloralose-anesthetized, vagotomized and aortic-denervated rabbits (n = 10), we recorded muscle SNA from tibial nerve by microneurography, simultaneously with renal and cardiac SNAs by wire electrode. To produce a baroreflex open-loop condition, we isolated the carotid sinuses from systemic circulation and altered the intracarotid sinus pressure (CSP) according to a binary white noise sequence of operating pressure ± 20 mmHg (for investigating dynamic characteristics of baroreflex) or in stepwise 20-mmHg increments from 40 to 160 mmHg (for investigating static characteristics of baroreflex). Dynamic high-pass characteristics of baroreflex control of muscle SNA, assessed by the increasing slope of transfer gain, showed that more rapid change of arterial pressure resulted in greater response of muscle SNA to pressure change and that these characteristics were similar to cardiac SNA but greater than renal SNA. However, numerical simulation based on the transfer function shows that the differences in dynamic baroreflex control at various organs result in detectable differences among SNAs only when CSP changes at unphysiologically high rates (i.e., 5 mmHg/s). On the other hand, static reverse-sigmoid characteristics of baroreflex control of muscle SNA agreed well with those of renal or cardiac SNAs. In conclusion, dynamic-linear and static-nonlinear baroreflex control of muscle SNA is similar to that of renal and cardiac SNAs under physiological pressure change.

carotid sinus pressure

ARTERIAL BAROREFLEX CONTROL of efferent sympathetic nerve activity (SNA) has a very important role in circulatory control (3, 23). It powerfully regulates arterial pressure and attenuates physiological perturbations in arterial pressure via the baroreflex feedback-loop system. Without the baroreflex control of SNA, the simple act of standing causes a great fall in arterial pressure, leading to hypoperfusion to the brain and sometimes loss of consciousness (3, 23). In addition, impaired baroreflex control of SNA may be associated with the pathophysiology of cardiovascular diseases (7, 8, 28). Accordingly, baroreflex control of SNA has been an important target in the studies of cardiovascular physiology and pathophysiology. In earlier studies addressing the baroreflex control of SNA in humans, SNA innervating vessels in skeletal muscles, termed muscle SNA, has been directly measured by microneurographic technique (16, 26, 29), and considered as a proxy of systemic SNA. These studies have contributed significantly to the understanding of the baroreflex control of SNA in circulatory physiology (5, 22, 24) [such as during exercise (4, 12, 25), hypoxia (9, 10), orthostasis (2), heating (13), and aging (17, 26, 27)] and pathophysiology [such as hypertension (7, 28), heart failure (8), myocardial infarction (6), obstructive sleep apnea (21), and neurally mediated syncope (19)].

Despite accumulated knowledge on baroreflex control of muscle SNA, whether the control of muscle SNA parallels that of other visceral organs innervated by the sympathetic nerve system, including the kidney and heart, remains unclear. This is because the human microneurographic technique is mainly limited to the upper and lower limbs (16, 18). Although earlier human studies reported that microneurographical muscle SNA correlated with norepinephrine spillovers in the kidney and heart at rest (30, 31), these studies did not assess baroreflex control of SNA. Because of a lack of definitive evidence, the impact of investigating baroreflex control of muscle SNA could be somewhat limited. Accordingly, we tested whether dynamic and static baroreflex control of muscle SNA is similar to that of renal and cardiac SNAs. We recorded muscle SNA by microneurography simultaneously with renal and cardiac SNAs in anesthetized rabbits. We then compared the dynamic-linear and static-nonlinear characteristics of baroreflex control for the three forms of SNAs.

MATERIALS AND METHODS

Preparation. Animals were cared for in strict accordance with the "Guiding Principles for the Care and Use of Animals in the Field of Physiological Science" approved by the Physiological Society of Japan. The experimental protocol was approved by the animal experiment committee of Japan Aerospace Exploration Agency. Ten Japanese white rabbits weighing 2.4–3.3 kg were initially anesthetized by intravenous injection (2 ml/kg) of a mixture of urethane (250 mg/ml) and α-chloralose (40 mg/ml). Anesthesia was maintained by continuously infusing the anesthetics at a rate of 0.33 $ml \cdot kg^{-1} \cdot h^{-1}$ using a syringe pump (CFV-3200, Nihon Kohden, Tokyo). The rabbits were

Address for reprint requests and other correspondence: A. Kamiya, Dept. of Cardiovascular Dynamics, National Cardiovascular Center Research Institute, 5-7-1 Fujishirodai, Suita, Osaka 565-8565, Japan (e-mail: kamiya@ri.ncvc.go.jp).

The costs of publication of this article were defrayed in part by the payment of page charges. The article must therefore be hereby marked "*advertisement*" in accordance with 18 U.S.C. Section 1734 solely to indicate this fact.

mechanically ventilated with oxygen-enriched room air. Bilateral carotid sinuses were isolated vascularly from the systemic circulation by ligating the internal and external carotid arteries and other small branches originating from the carotid sinus regions. The isolated carotid sinuses were filled with warmed physiological saline pre-equilibrated with atmospheric air through catheters inserted via the common carotid arteries. The intracarotid sinus pressure (CSP) was controlled by a servo-controlled piston pump (model ET-126A, Labworks; Costa Mesa, CA). Bilateral vagal and aortic depressor nerves were sectioned in the middle of the neck region to eliminate reflexes from the cardiopulmonary region and the aortic arch. The systemic arterial pressure (AP) was measured using a high-fidelity pressure transducer (Millar Instruments; Houston, TX) inserted retrogradely from the right common carotid artery below the isolated carotid sinus region. Body temperature was maintained at ~38°C with a heating pad.

The left renal sympathetic nerve was exposed retroperitoneally, and the left cardiac sympathetic nerve was exposed through a middle thoracotomy. A pair of stainless steel wire electrodes (Bioflex wire AS633, Cooner Wire) was attached to each of these nerves to record renal and cardiac SNAs. The left tibial nerve was exposed at the right popliteal fossa through incising the flexors in the dorsal middle region of the thigh. A tungsten microelectrode (model 26–05-1, Frederick Haer; Bowdoinham, ME) was inserted into the right tibial nerve to record muscle SNA, based on human (16, 26) and animal (20) microneurography. We identified muscle SNA by the following discharge characteristics: *1*) afferent activity induced by tapping of the calf muscles but not by gently touching the skin, and *2*) excitatory and inhibitory responses induced by decreasing and increasing CSP, respectively.

The nerve fibers peripheral to electrodes were ligated securely and crushed to eliminate afferent signals. The nerve and electrodes were covered with a mixture of silicone gel (Silicon Low Viscosity, KWIK-SIL, World Precision Instrument) to insulate and immobilize the electrodes. The preamplified SNA signals were band-pass filtered at 150–1,000 Hz. These nerve signals were full-wave rectified and low-pass filtered with a cutoff frequency of 30 Hz to quantify the nerve activity.

Evaluation of baroreflex control of SNA: dynamic-linear and static nonlinear characteristics. Baroreflex controls of cardiac and renal SNAs have dynamic-linear high-pass and static-nonlinear reverse-sigmoidal characteristics (14). The dynamic high-pass characteristics indicate that more rapid change of arterial pressure is associated with greater SNA response. Identifying the transfer function from baroreceptor pressure input to SNA is the most powerful tool to quantify dynamic-linear characteristics. Importantly, the transfer function can predict linear SNA responses to any baroreceptor pressure input. On the other hand, the baroreflex control also has static-nonlinear reverse-sigmoidal characteristics that cannot be explained by dynamic-linear characteristics, particularly under steady-state condition (14). Accordingly, we evaluated baroreflex control of SNA by assessing both dynamic-linear and static-nonlinear characteristics while opening the baroreflex feedback loop independently for muscle, cardiac, and renal SNAs.

Protocols. After the surgical preparation, the rabbit was maintained supine. *Protocols 1* and *2* described below were conducted to assess static-nonlinear and dynamic-linear characteristics, respectively, in randomized order with an interval of at least 5 min. Both protocols were conducted in all animals ($n = 10$). In both protocols, bilateral CSP was controlled by a servo-controlled piston pump (14).

In *protocol 1*, CSP was increased stepwise from 40 to 160 mmHg in increments of 20 mmHg. Each pressure step was maintained for 60 s. The three SNAs, CSP, and AP were recorded for 7 min at a sampling rate of 200 Hz using a 12-bit analog-to-digital converter. Data were stored on the hard disk of a dedicated laboratory computer system.

In *protocol 2*, CSP was first matched with systemic AP to obtain the operating AP under the baroreflex closed-loop condition. After at least 5 min of stabilization, the three SNAs, CSP, and AP were recorded for 10 min and stored as in *protocol 1*. The average AP over 10 min was defined as the operating AP. Then, after at least 5 min of stabilization, CSP was randomly assigned at 20 mmHg above or below the operating AP every 500 ms according to a binary white noise sequence in which the input power spectrum of CSP was reasonably flat up to 1 Hz (14). The three SNAs, CSP, and AP were recorded for 10 min and stored for analysis.

Data analysis. SNA signals were normalized by the following steps. First, for each type of SNA, 0 arbitrary unit (au) was assigned to the postmortem noise level. Second, SNA signals were averaged for the last 10 s at CSP level of 40 mmHg in *protocol 1*; 100 au were then assigned to the average SNA. Last, the other SNA signals in both *protocols 1* and *2* were then normalized to these values.

In *protocol 1*, muscle, renal and cardiac SNAs were averaged for the last 10 s of each CSP level. The static-nonlinear relation between CSP and each SNA was parameterized using a four-parameter logistic equation model as follows:

$$\mathrm{SNA} = P_4 + \frac{P_1}{1 + \exp[P_2(\mathrm{CSP} - P_3)]} \quad (1)$$

where P_1 is the response range of SNA (i.e., the difference between the maximum and minimum SNA), P_2 is the coefficient of gain, P_3 is the midpoint CSP of the logistic function, and P_4 is the minimum SNA. We calculated the instantaneous gain from the first derivative of the logistic function, and the maximum gain from $-P_1P_2/4$ at $x = P_3$.

In *protocol 2*, we calculated the transfer (the gain and phase) and coherence functions from CSP input to each SNA. We resampled CSP and SNA at 10 Hz and segmented them into 10 sets of 50% overlapping bins of 2^{10} data points each. The segment length was 102.4 s, which yielded the lowest frequency bound of 0.01 (0.0097) Hz. We subtracted a linear trend and applied a Hanning window for each segment. We then performed fast Fourier transform to obtain frequency spectra of CSP and SNA. We ensemble-averaged the CSP power [$Sxx(f)$], SNA power [$Syy(f)$], and cross power between CSP and SNA [$Syx(f)$] over the 10 segments. Thereafter, we calculated the transfer function [$H(f)$] from CSP to SNA as follows

$$H(f) = \frac{Syx(f)}{Sxx(f)} \quad (2)$$

To quantify the linear dependence between CSP and SNA in the frequency domain, we calculated the magnitude-squared coherence function [$\mathrm{Coh}(f)$] as follows

$$\mathrm{Coh}(f) = \frac{|Syx(f)|^2}{Sxx(f)Syy(f)} \quad (3)$$

The coherence value ranges from zero to unity. Unity coherence indicates a perfect linear dependence between CSP and SNA, whereas zero coherence indicates total independence of these two signals.

Statistical analysis. All data are presented as means ± SD. We used a repeated-measures analysis of variance with post hoc multiple comparisons to compare variables among muscle, renal, and cardiac SNAs. Differences were considered significant when $P < 0.05$.

RESULTS

Static baroreflex characteristics (protocol 1). Muscle SNA decreased in response to stepwise increase in CSP in *protocol 1*. The change in muscle SNA appeared similar to that in renal or cardiac SNA (Fig. 1). The relation between CSP and muscle SNA was fitted to four-parameter logistic function in individual animals. The fitted logistic function of muscle SNA almost superimposed that of renal or cardiac SNA (Fig. 2). The

parameters of P_1, P_2, P_3, and P_4 and the maximal gain (at the midpoint of the sigmoid curve) of muscle SNA were similar to those of renal or cardiac SNA (Fig. 2, Table 1).

Dynamic baroreflex characteristics (protocol 2). In *protocol 2*, the CSP was perturbed according to a binary white noise sequence at 500-ms intervals (Fig. 3). When CSP was increased, muscle SNA decreased, and vice versa. Although the shape of each burst of muscle SNA differed from that of renal or cardiac SNA, the global characteristics of dynamic changes of muscle SNA appeared roughly the same as those of renal and cardiac SNAs.

In a frequency domain analysis (Fig. 4*A*), the gain of the transfer function from CSP to muscle SNA increased as the frequency of CSP perturbation increased between 0.01 and 0.8 Hz, indicating dynamic high-pass characteristics. The transfer gains in renal and cardiac SNAs also showed high-pass characteristics. The increasing slope of the gain between 0.01 and 0.8 Hz for muscle SNA was similar to that for cardiac SNA but steeper than that for renal SNA (Fig. 4*A*, Table 2). The gains between 0.3 and 1 Hz of muscle SNA were similar to those of cardiac SNA but greater than those of renal SNA ($P < 0.05$) (Table 2).

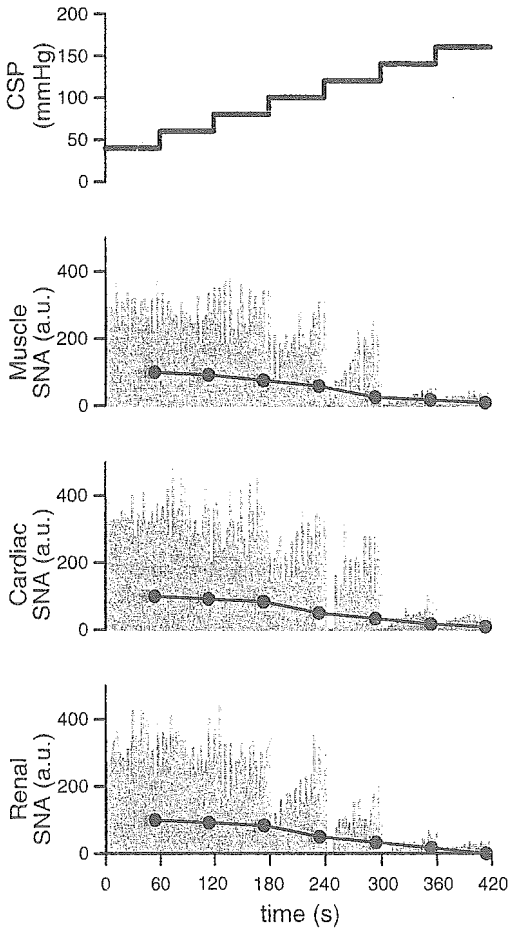

Fig. 1. Representative data of one rabbit in *protocol 1*, showing integrated signals of muscle, cardiac, and renal sympathetic nerve activity (SNA) during stepwise increase in carotid sinus pressure (CSP). Each step is 60 s. Fine lines indicate SNA signals resampled at 10 Hz. Bold lines and closed circles indicate SNA signals averaged over the last 10 s of each CSP level, which were used to determine the static nonlinear characteristics of baroreflex control of each SNA. au, Arbitrary unit.

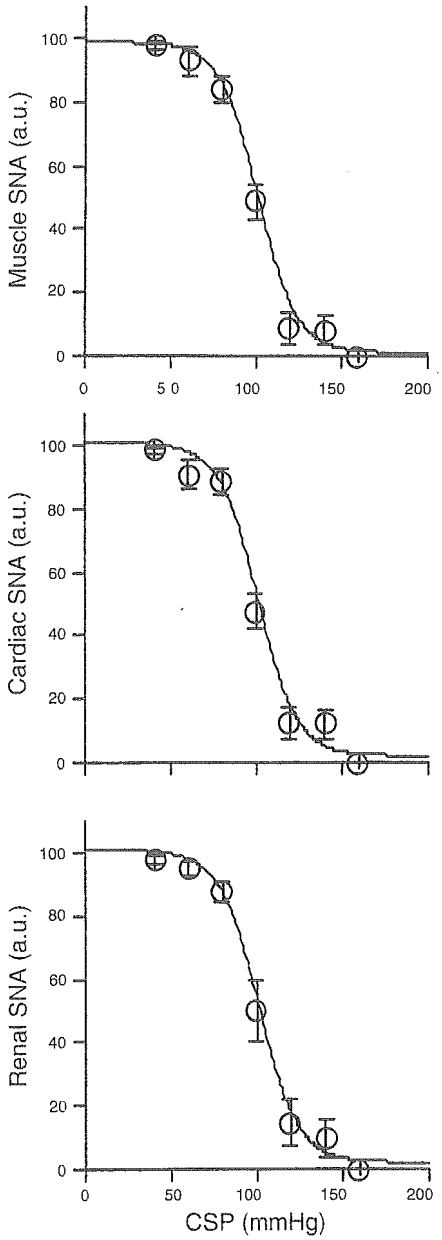

Fig. 2. Static nonlinear, reverse-sigmoidal baroreflex relationship between each SNA (muscle, cardiac, and renal SNA) and CSP from all animals (n = 10) in *protocol 2*. ○, Mean SNA. Error bars denote SD. The static nonlinear characteristics of muscle SNA were similar to those of cardiac and renal SNAs.

The phase of the transfer function from CSP to muscle SNA lagged as frequency increased (Fig. 4*A*), and the frequency-dependent lag was slightly greater than cardiac and renal SNAs. The phase of muscle SNA showed greater lag than that of cardiac SNA from 0.1 to 1 Hz ($P < 0.05$) and than that of renal SNA at 1 Hz ($P < 0.05$) (Table 2).

The coherence of the transfer function from CSP to muscle SNA was over 0.8 between 0.1 and 0.8 Hz, except at ~0.35 Hz (Fig. 4*A*). The coherence of muscle SNA was greater than that of cardiac and renal SNAs at 0.1, 0.8, and 1 Hz ($P < 0.05$) (Table 2).

The step response of muscle SNA to CSP consisted of an initial decrease followed by partial recovery and then steady state (Fig. 4*B*). The initial decrease in muscle SNA was similar

to that in cardiac SNA but greater than that in renal SNA (Fig. 4*B*, Table 2). However, steady-state muscle SNA was similar to that of cardiac and renal SNAs (Fig. 4*B*, Table 2).

DISCUSSION

Despite accumulated knowledge on baroreflex control of muscle SNA, whether the baroreflex control of muscle SNA parallels that of other visceral organs innervated by the sympathetic nervous system, including the kidney and heart, remains unclear. This study has two major new findings. First, the dynamic high-pass characteristic of baroreflex control for muscle SNA, assessed by the increasing slope of transfer gain, is similar to that of cardiac SNA but greater than that of renal SNA. However, the difference is physiologically insignificant, because it may induce detectable differences among SNAs only when AP changes at unphysiologically high rates (see below). Second, the static reverse-sigmoidal relationship between CSP and muscle SNA is almost identical to that of both cardiac and renal SNAs. These findings support our hypothesis to a large extent and indicate that dynamic-linear and static-nonlinear baroreflex control of muscle SNA is similar to that of renal and cardiac SNAs under physiological pressure changes.

The present study quantified the dynamic high-pass characteristics of baroreflex control of muscle SNA by opening the baroreflex feedback loop. In humans, responses of muscle SNA to change in AP is believed to depend on the speed of AP change; more rapid AP change is associated with greater muscle SNA response to AP change. This suggests the presence of high-pass characteristics in the baroreflex control of muscle SNA, and this was actually found in previous human study by sinusoidal modulation of muscle SNA by neck suction at varying frequencies (1). We investigated the transfer function in animals and showed that the transfer gain increased as the frequency of CSP perturbation increased when the increasing slope of transfer gain was 1.84 dB/octave (Table 2). This finding indicates that when CSP changes more rapidly with doubling of the frequency, SNA response increases 1.24 times. In addition, our calculated step response from high-pass transfer function (initial decrease followed by partial recovery, Fig. 4*B*) agrees with the time series of human muscle SNA observed during graded neck pressure or suction (22), supporting the validity of our system identification.

Our data revealed that the dynamic high-pass characteristics of baroreflex control of muscle SNA are similar to those of cardiac SNA but greater than those of renal SNA. In other words, more rapid AP change results in greater muscle SNA in response to pressure change, and this characteristic is similar to cardiac SNA but stronger than renal SNA. Quantitative estimation from the increasing slopes of transfer gain (Table 2) indicates that when the frequency of CSP doubles, the response of cardiac SNA response increases 1.30 times, which is statistically similar to muscle SNA (1.24 times), whereas the response of renal SNA increases 1.13 times and is lower than the muscle and cardiac SNAs. The difference between cardiac and renal SNAs is consistent with previous study (14).

Numerical simulation based on the transfer function estimated by *protocol 2* shows that the differences in dynamic baroreflex control in various organs induce detectable differences among SNAs only when AP changes at very high rates (Fig. 5). According to our previous studies (15), we modeled transfer function of baroreflex control of SNA (see APPENDIX) by setting the parameters of the function to reflect our actual data. The numerical simulation shows that the faster the increasing speed of CSP, the more prominent are the differences among the responses of three SNAs; muscle and cardiac SNAs decrease more markedly than renal SNA (Fig. 5, compare *D*

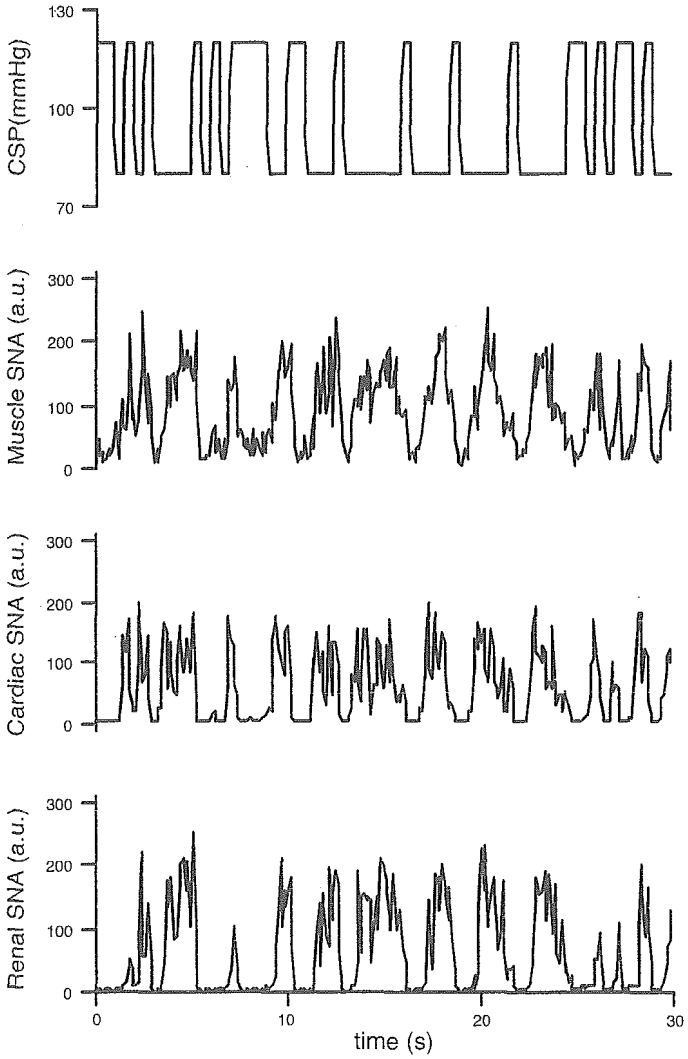

Fig. 3. Representative data of 1 rabbit in *protocol 2*, showing time series of CSP and muscle, cardiac, and renal SNA during CSP perturbation. CSP was changed according to a binary white noise signal with a switching interval of 500 ms.

Table 1. *Four-parameter logistic function fitted to static nonlinear characteristics of baroreflex control of SNA: muscle SNA vs. renal and cardiac SNAs*

	Muscle SNA	Cardiac SNA	Renal SNA
P_1, au	99±1	99±1	98±1
P_2, au/mmHg	0.12±0.02	0.13±0.03	0.12±0.01
P_3, mmHg	102±4	101±4	101±4
P_4, au	0.1±0.3	0.1±0.3	0.1±0.3
G_{max}, au/mmHg	−2.9±0.4	−3.3±0.5	−2.8±0.3

Values are means ± SD (n = 10). See *Eq. 1* in MATERIALS AND METHODS for definition of the 4 parameters (P_1–P_4) of logistic function. All parameters of muscle sympathetic nerve activity (SNA) are similar to those of renal and cardiac SNAs. G_{max}, maximum gain.

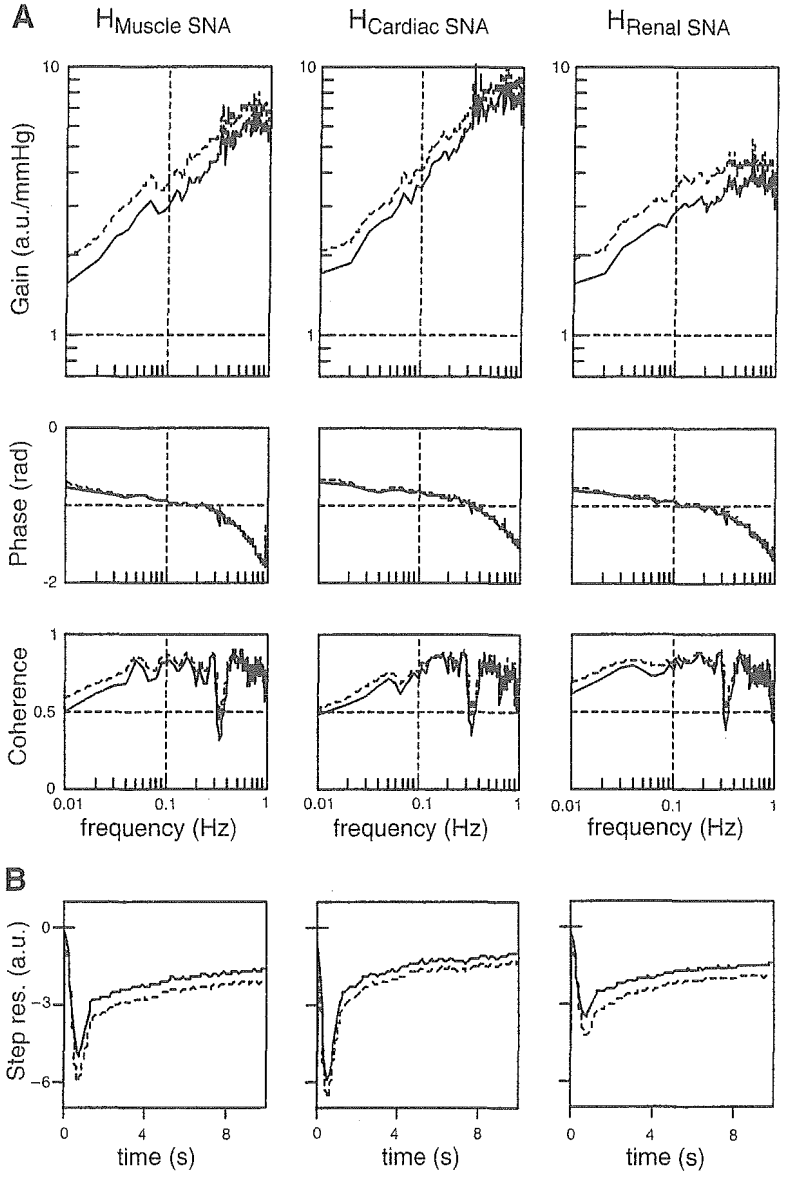

Fig. 4. *A*: transfer function from CSP to renal SNA ($H_{RenalSNA}$), to cardiac SNA ($H_{CardiacSNA}$) and to muscle SNA ($H_{MuscleSNA}$) from all animals (n = 10) in *protocol 2*. Gain plots (*top*), phase plots (*middle*), and coherence function (*bottom*) are shown. Slope of the transfer gain increases more markedly in $H_{MuscleSNA}$ and $H_{CardiacSNA}$ than in $H_{RenalSNA}$. *B*: step responses (Step res) derived from $H_{RenalSNA}$, $H_{CardiacSNA}$, and $H_{MuscleSNA}$. Solid and dashed lines represent mean and mean + SD values, respectively.

and *C* to *B*). However, the organ-dependent differences become detectable only when CSP increases at a high speed of 5 mmHg/s. In clinical situation, AP hardly increases at such high rates even with pharmacological intervention in medical treatment; therefore these SNAs may be similar under physiological pressure changes. Moreover, even if CSP increases at a very high rate, the three SNAs reach similar steady-state activities, reflecting their similar transfer gains at the lowest frequency (Fig. 4*A*, Table 1).

We rigorously investigated the static nonlinear characteristics of baroreflex control of muscle SNA from the relationship between steady-state values of CSP and muscle SNA. Although earlier human studies addressed the reverse-sigmoidal relationship of baroreflex control of muscle SNA using conventional open-loop condition by neck suction and pressure (22) as well as pharmacological (i.e., administration of phenylephrine and nitroprusside) methods (24), these studies failed to determine the relationship in individual subjects. In addition, because these studies analyzed the relationship based on data of dynamically changing SNA in response to changing baroreceptor pressure and not steady-state SNA at constant pressure, the relationship derived should include dynamic linear characteristics of baroreflex control of SNA, and pure static nonlinear characteristics could not be extracted. Given the presence of dynamic characteristics, determining steady-state relationship between SNA and baroreceptor pressure requires keeping the baroreceptor pressure constant until SNA reaches the steady-state level. In the present study (*protocol 1*), we determined the relationship between muscle SNA and CSP at approximately steady state in individual animals.

Our data indicate that static nonlinear characteristics of baroreflex control of muscle SNA are almost identical to those of renal and cardiac SNAs. This finding indicates that steady-state muscle SNA approximates that of renal and cardiac SNA at any baroreceptor pressure. This finding is consistent with the calculated step response of SNA to CSP change (Fig. 4*B*) because muscle SNA reaches the steady-state level similar in magnitude to cardiac and renal SNAs despite differences in the initial rapid decreases at the three sites. This also agrees with the numerical simulation (Fig. 5, *B–D*), which reveals that

Table 2. *Transfer function of baroreflex control of SNA (from CSP to SNA): muscle SNA vs. renal and cardiac SNAs*

	Muscle SNA	Cardiac SNA	Renal SNA
Gain, au/mmHg			
0.01 Hz	1.59±0.39	1.69±0.53	1.56±0.35
0.1 Hz	3.10±0.46	3.48±0.47	2.90±0.43
0.3 Hz	4.36±0.48	5.75±0.41	3.28±0.43*†
0.8 Hz	6.11±0.66	7.71±0.60	3.50±0.44*†
1.0 Hz	5.17±0.72	6.87±0.60	3.02±0.69*†
Phase, rad			
0.01 Hz	−2.34±0.16	−2.29±0.10	−2.51±0.13
0.1 Hz	−2.86±0.04	−2.58±0.04*	−2.92±0.05†
0.3 Hz	−3.48±0.10	−2.98±0.04*	−3.41±0.09†
0.8 Hz	−5.09±0.10	−4.31±0.10*	−4.73±0.10†
1.0 Hz	−5.67±0.10	−4.94±0.09*	−5.30±0.10*†
Coherence			
0.01 Hz	0.52±0.09	0.52±0.03	0.65±0.07
0.1 Hz	0.83±0.03	0.72±0.04*	0.77±0.03*
0.3 Hz	0.83±0.04	0.87±0.02	0.88±0.02
0.8 Hz	0.82±0.03	0.75±0.03*	0.72±0.04*
1.0 Hz	0.61±0.07	0.52±0.08*	0.52±0.08*
Slope, dB/octave (0.01–0.8 Hz)	1.84±0.44	2.28±0.48	1.08±0.18*†
Step response, au			
Initial response	−5.04±0.75	−5.70±0.71	−3.53±0.71*†
Steady-state level	−1.54±0.32	−1.19±0.28	−1.46±0.32

Values are means ± SD (n = 10). CSP, intracarotid sinus pressure. *P < 0.05, muscle SNA vs. renal SNA or cardiac SNA. †P < 0.05, renal SNA vs. cardiac SNA.

these SNAs reach similar steady-state levels even though they respond differently to CSP increase.

The present study may extend earlier studies investigating the relationship between muscle SNA and other SNAs innervating visceral organs (30, 31). These studies reported that microneurographical muscle SNA correlated with norepinephrine spillovers in the heart at rest, handgrip, and mental stress (30), and those in the kidney at rest (31). Although these studies suggested a correlation between muscle SNA and cardiac or renal SNA, they did not assess baroreflex control of SNA. In addition, the spillover measurements may be affected by neurotransmitter kinetics in synapses (release and uptake) and circulating norepinephrine independent of SNA (11), and the method has a low time resolution for assessing the dynamic baroreflex control of SNA. Accordingly, we measured the three SNAs directly and investigated the baroreflex control of each SNA.

Limitations. The present study has several limitations. First, we excluded the efferent effect of vagally mediated arterial baroreflex, which could affect the properties of baroreflex control of SNAs. Second, artificial respiration and surgical procedures used in this study could affect baroreflex. Third, anesthetic agents tend to inhibit efferent SNA and depress the gain of baroreflex control of SNA. Fourth, we used physiological saline preequilibrated with atmospheric air to perfuse the carotid sinuses. Local hypoxia could have occurred and somewhat affected baroreflex control of SNA. Last, although we

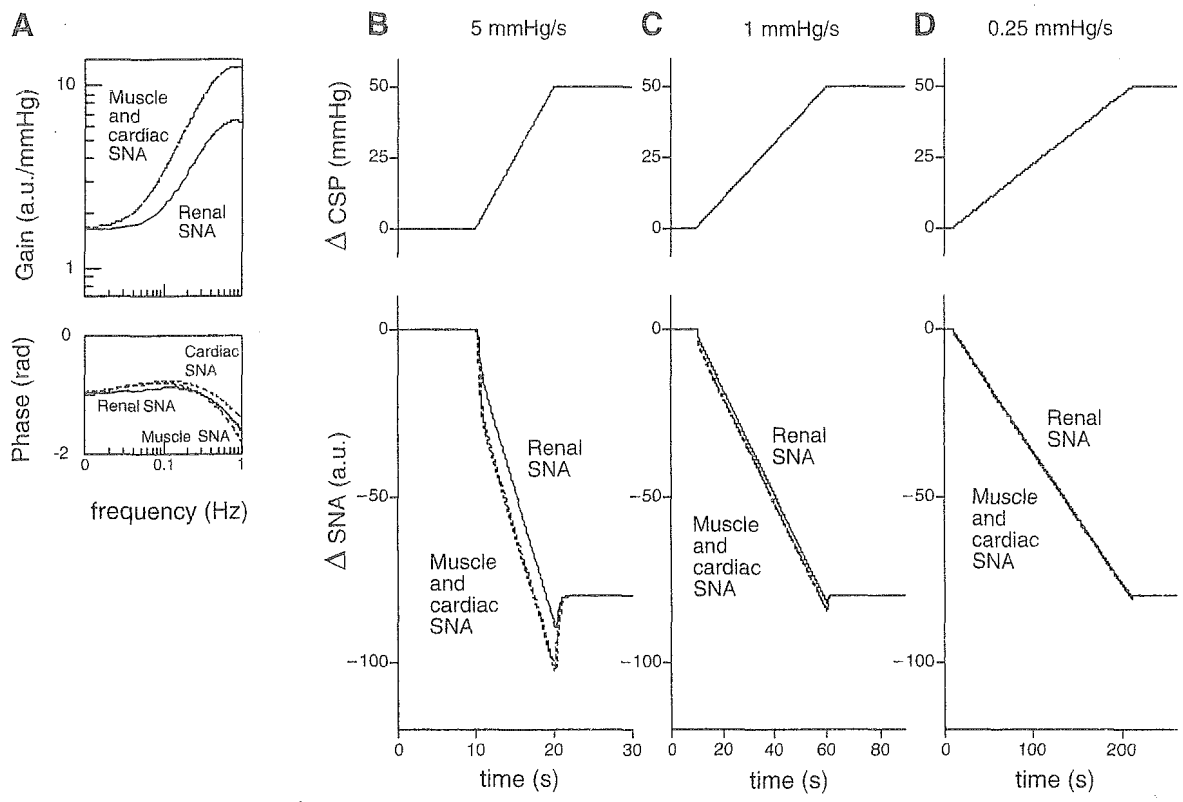

Fig. 5. Simulation of muscle, cardiac, and renal SNA in response to rapid (*B*), moderate (*C*) and slow (*D*) ramp increase in CSP. On the basis of the data from *protocol 2*, the transfer function of baroreflex control of SNA (from CSP input to SNA) is modeled (*A*) as described in APPENDIX. In all panels (except CSP panels), solid, thin dashed, and dashed lines represent the simulation for muscle, cardiac, and renal SNA, respectively. Data of cardiac SNA almost overlap with those of muscle SNA (except Phase panel in *A*). When CSP increases more rapidly (*B*), muscle and cardiac SNAs decrease in response to CSP change more markedly than renal SNA. Of note, time axes are different among panels. The slower the increasing speed of CSP, the smaller the difference among responses of 3 SNAs (*C* and *D*). Despite the difference in dynamic responses, however, all SNAs reach similar steady-state activity levels, regardless of the CSP increasing speed.

held CSP for 60 s at each CSP level in *protocol 1*, some SNAs did not reach steady-state level within 60 s (Fig. 1). Therefore, the duration may be short to obtain steady-state SNA in all cases. However, because holding CSP for longer periods can induce SNA changes originating from factors other than CSP change itself, it is difficult to know precisely when SNA reaches steady-state level. Future study is needed to examine pure static baroreflex characteristics.

In summary, dynamic high-pass characteristics of baroreflex control of muscle SNA, assessed by the increasing slope of transfer gain, showed that more rapid change of arterial pressure resulted in greater response of muscle SNA to pressure change and that these characteristics were similar to cardiac SNA but greater than renal SNA. However, the numerical simulation based on the transfer function shows that the differences in dynamic baroreflex control at various organs result in detectable difference among SNAs only when AP changes at unphysiologically high rates (i.e., 5 mmHg/s). In addition, static reverse-sigmoid characteristics of baroreflex control of muscle SNA are almost identical with those of renal or cardiac SNAs. We conclude that dynamic-linear and static-nonlinear baroreflex control of muscle SNA is similar to that of renal and cardiac SNAs, with the exception of a mildly reduced dynamic-linear response of renal SNA to rapid pressure change outside the physiological range.

APPENDIX

In rabbits, the transfer function of the baroreflex neural arc (baroreceptor pressure to SNA) approximates derivative characteristics in the frequency range below 0.8 Hz and high-cut characteristics of frequencies above 0.8 Hz (15). Therefore, according to our previous study (15), we model the neural arc transfer function (H_N) using *Eq. A1* as follows

$$H_N(f) = -K_N \frac{1+\frac{f}{f_{c1}}j}{\left(1+\frac{f}{f_{c2}}\right)^2}\exp(-2\pi fjL) \qquad (A1)$$

where f and j represent the frequency (in Hz) and imaginary units, respectively; K_N is static gain (in au/mmHg); f_{c1} and f_{c2} ($f_{c1} < f_{c2}$) are corner frequencies (in Hz) for derivative and high-cut characteristics, respectively; and L is a pure delay (in s) that would represent the sum of delays in the synaptic transmission at the baroreflex central pathways and the sympathetic ganglion. The dynamic gain increases in the frequency range from f_{c1} to f_{c2} and decreases above f_{c2}. On the basis of the measured results from *protocol 1*, we set K_N at 1.6 and f_{c2} at 0.8 similarly in all of muscle, cardiac, and renal SNAs in simulations shown in Fig. 5. In addition, we set f_{c1} at 0.05, 0.05, and 0.1, respectively, in muscle, cardiac and renal SNA. We also set L at 0.3, 0.1 and 0.2, respectively, corresponding to the distance of neural pathway from carotid sinus region to the tibial, cardiac, and renal sympathetic nerve.

GRANTS

This study is a part of the "Ground-Based Research Announcement for Space Utilization" project promoted by Japan Space Forum. This study was also supported by Industrial Technology Research Grant Program 03A47075 from New Energy and Industrial Technology Development Organization (NEDO) of Japan.

REFERENCES

1. **Bernardi L, Hayoz D, Wenzel R, Passino C, Calciati A, Weber R, and Noll G.** Synchronous and baroceptor-sensitive oscillations in skin microcirculation: evidence for central autonomic control. *Am J Physiol Heart Circ Physiol* 273: H1867–H1878, 1997.
2. **Cooke WH, Hoag JB, Crossman AA, Kuusela TA, Tahvanainen KU, and Eckberg DL.** Human responses to upright tilt: a window on central autonomic integration. *J Physiol* 517: 617–628, 1999.
3. **Eckberg DL and Sleight P.** *Human Baroreflexes in Health and Disease.* New York: Oxford Univ. Press, 1992.
4. **Fadel PJ, Ogoh S, Watenpaugh DE, Wasmund W, Olivencia-Yurvati A, Smith ML, and Raven PB.** Carotid baroreflex regulation of sympathetic nerve activity during dynamic exercise in humans. *Am J Physiol Heart Circ Physiol* 280: H1383–H1390, 2001.
5. **Furlan R, Diedrich A, Rimoldi A, Palazzolo L, Porta C, Diedrich L, Harris PA, Sleight P, Biagioni I, Robertson D, and Bernardi L.** Effects of unilateral and bilateral carotid baroreflex stimulation on cardiac and neural sympathetic discharge oscillatory patterns. *Circulation* 108: 717–723, 2003.
6. **Graham LN, Smith PA, Stoker JB, Mackintosh AF, and Mary DA.** Time course of sympathetic neural hyperactivity after uncomplicated acute myocardial infarction. *Circulation* 106: 793–797, 2002.
7. **Grassi G, Cattaneo BM, Seravalle G, Lanfranchi A, and Mancia G.** Baroreflex control of sympathetic nerve activity in essential and secondary hypertension. *Hypertension* 31: 68–72, 1998.
8. **Grassi G, Seravalle G, Cattaneo BM, Lanfranchi A, Vailati S, Giannattasio C, Del Bo A, Sala C, Bolla GB, and Pozzi M.** Sympathetic activation and loss of reflex sympathetic control in mild congestive heart failure. *Circulation* 92: 3206–3211, 1995.
9. **Halliwill JR, Morgan BJ, and Charkoudian N.** Peripheral chemoreflex and baroreflex interactions in cardiovascular regulation in humans. *J Physiol* 552: 295–302, 2003.
10. **Hansen J and Sander M.** Sympathetic neural overactivity in healthy humans after prolonged exposure to hypobaric hypoxia. *J Physiol* 546: 921–929, 2003.
11. **Jennings GL.** Noradrenaline spillover and microneurography measurements in patients with primary hypertension. *J Hypertens Suppl* 16: S35–S38, 1998.
12. **Kamiya A, Michikami D, Fu Q, Niimi Y, Iwase S, Mano T, and Suzumura A.** Static handgrip exercise modifies arterial baroreflex control of vascular sympathetic outflow in humans. *Am J Physiol Regul Integr Comp Physiol* 281: R1134–R1139, 2001.
13. **Kamiya A, Michikami D, Hayano J, and Sunagawa K.** Heat stress modifies human baroreflex function independently of heat-induced hypovolemia. *Jpn J Physiol* 53: 215–222, 2003.
14. **Kawada T, Shishido T, Inagaki M, Tatewaki T, Zheng C, Yanagiya Y, Sugimachi M, and Sunagawa K.** Differential dynamic baroreflex regulation of cardiac and renal sympathetic nerve activities. *Am J Physiol Heart Circ Physiol* 280: H1581–H1590, 2001.
15. **Kawada T, Zheng C, Yanagiya Y, Uemura K, Miyamoto T, Inagaki M, Shishido T, Sugimachi M, and Sunagawa K.** High-cut characteristics of the baroreflex neural arc preserve baroreflex gain against pulsatile pressure. *Am J Physiol Heart Circ Physiol* 282: H1149–H1156, 2002.
16. **Mano T.** Microneurography as a tool to investigate sympathetic nerve responses to environmental stress. *Aviakosmicheskaia Ekologicheskaia Meditsina* 31: 8–14, 1997.
17. **Markel TA, Daley JC III, Hogeman CS, Herr MD, Khan MH, Gray KS, Kunselman AR, and Sinoway LI.** Aging and the exercise pressor reflex in humans. *Circulation* 107: 675–678, 2003.
18. **Mitchell JH and Victor RG.** Neural control of the cardiovascular system: insights from muscle sympathetic nerve recordings in humans. *Med Sci Sports Exerc* 28: S60–S69, 1996.
19. **Mosqueda-Garcia R, Furlan R, Tank J, and Fernandez-Violante R.** The elusive pathophysiology of neurally mediated syncope. *Circulation* 102: 2898–2906, 2000.
20. **Nakamura T, Kawahara K, Kusunoki M, and Feng Z.** Microneurography in anesthetized rats for the measurement of sympathetic nerve activity in the sciatic nerve. *J Neurosci Methods* 131: 35–39, 2003.
21. **Narkiewicz K, Pesek CA, Kato M, Phillips BG, Davison DE, and Somers VK.** Baroreflex control of sympathetic nerve activity and heart rate in obstructive sleep apnea. *Hypertension* 32: 1039–1043, 1998.
22. **Rea RF and Eckberg DL.** Carotid baroreceptor-muscle sympathetic relation in humans. *Am J Physiol Regul Integr Comp Physiol* 253: R929–R934, 1987.

23. **Rowell LB.** *Human Cardiovascular Control.* New York: Oxford Univ. Press, 1993.
24. **Rudas L, Crossman AA, Morillo CA, Halliwill JR, Tahvanainen KU, Kuusela TA, and Eckberg DL.** Human sympathetic and vagal baroreflex responses to sequential nitroprusside and phenylephrine. *Am J Physiol Heart Circ Physiol* 276: H1691–H1698, 1999.
25. **Scherrer U, Pryor SL, Bertocci LA, and Victor RG.** Arterial baroreflex buffering of sympathetic activation during exercise-induced elevations in arterial pressure. *J Clin Invest* 86: 1855–1861, 1990.
26. **Sundlof G and Wallin BG.** Human muscle nerve sympathetic activity at rest. Relationship to blood pressure and age. *J Physiol* 274: 621–637, 1978.
27. **Tanaka H, Davy KP, and Seals DR.** Cardiopulmonary baroreflex inhibition of sympathetic nerve activity is preserved with age in healthy humans. *J Physiol* 515: 249–254, 1999.
28. **Van De Borne P, Mezzetti S, Montano N, Narkiewicz K, Degaute JP, and Somers VK.** Hyperventilation alters arterial baroreflex control of heart rate and muscle sympathetic nerve activity. *Am J Physiol Heart Circ Physiol* 279: H536–H541, 2000.
29. **Wallin BG and Eckberg DL.** Sympathetic transients caused by abrupt alterations of carotid baroreceptor activity in humans. *Am J Physiol Heart Circ Physiol* 242: H185–H190, 1982.
30. **Wallin BG, Esler M, Dorward P, Eisenhofer G, Ferrier C, Westerman R, and Jennings G.** Simultaneous measurements of cardiac noradrenaline spillover and sympathetic outflow to skeletal muscle in humans. *J Physiol* 453: 45–58, 1992.
31. **Wallin BG, Thompson JM, Jennings GL, and Esler MD.** Renal noradrenaline spillover correlates with muscle sympathetic activity in humans. *J Physiol* 491: 881–887, 1996.

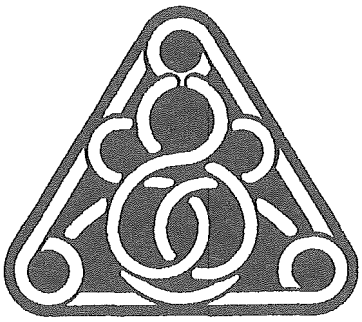

Reprinted from CIRCULATION, Volume 112, Number 3, July 19, 2005
Lippincott Williams & Wilkins Printed in U S A

Muscle Sympathetic Nerve Activity Averaged Over 1 Minute Parallels Renal and Cardiac Sympathetic Nerve Activity in Response to a Forced Baroreceptor Pressure Change

Atsunori Kamiya, MD, PhD; Toru Kawada, MD, PhD; Kenta Yamamoto, PhD,
Daisaku Michikami, PhD, Hideto Ariumi, PhD; Tadayoshi Miyamoto, PhD, Kazunori Uemura, MD;
Masaru Sugimachi, MD, PhD, Kenji Sunagawa, MD, PhD

Muscle Sympathetic Nerve Activity Averaged Over 1 Minute Parallels Renal and Cardiac Sympathetic Nerve Activity in Response to a Forced Baroreceptor Pressure Change

Atsunori Kamiya, MD, PhD; Toru Kawada, MD, PhD; Kenta Yamamoto, PhD; Daisaku Michikami, PhD; Hideto Ariumi, PhD; Tadayoshi Miyamoto, PhD; Kazunori Uemura, MD; Masaru Sugimachi, MD, PhD; Kenji Sunagawa, MD, PhD

Background—Despite the accumulated knowledge of human muscle sympathetic nerve activity (SNA) as measured by microneurography, whether muscle SNA parallels renal and cardiac SNAs remains unknown.

Method and Results—In experiment 1, muscle (microneurography, tibial nerve), renal, and cardiac SNAs were recorded in anesthetized rabbits (n=6) while arterial pressure was changed by intravenous bolus injections of nitroprusside (3 μg/kg) followed by phenylephrine (3 μg/kg). In experiment 2, the carotid sinus region was vascularly isolated in anesthetized, vagotomized, and aorta-denervated rabbits (n=10). The 3 SNAs were recorded while intracarotid sinus pressure was increased stepwise from 40 to 160 mm Hg in 20-mm Hg increments maintained for 60 seconds each. Muscle SNA averaged over 1 minute was well correlated with renal (r=0.96±0.01, mean±SE) and cardiac (r=0.96±0.01) SNAs in experiment 1 (baroreflex closed-loop condition) and also with renal (r=0.97±0.01) and cardiac (r=0.97±0.01) SNAs in experiment 2 (baroreflex open-loop condition).

Conclusions—Muscle SNA averaged over 1 minute parallels renal and cardiac SNAs in response to a forced baroreceptor pressure change. (***Circulation.* 2005;112:384-386.**)

Key Words: catecholamines ■ muscles ■ nervous system, autonomic ■ nervous system, sympathetic

Sympathetic nerve activity (SNA) plays a crucial role in controlling circulation both in healthy humans and in patients with cardiovascular diseases.[1] Activation of SNA increases heart rate, cardiac contractility, peripheral vascular resistance, and arterial pressure. Pathologically elevated SNA worsens survival in chronic heart failure and can induce lethal arrhythmias. Therefore, SNA has been an important target in the study of cardiovascular physiology and pathophysiology. In humans, activities of sympathetic nerves innervating blood vessels in skeletal muscles (muscle SNA) have been measured directly by microneurographic techniques[2–4] and considered a proxy of systemic SNA. Those studies have contributed greatly to the understanding of the significance of SNA in circulatory physiology[5] (including exercise,[6] aging,[7,8] and baroreflex[9]) and pathophysiology (including hypertension,[10] heart failure,[11] myocardial infarction,[12] and neurally mediated syncope[13]).

Despite the accumulated knowledge about muscle SNA, whether muscle SNA parallels other SNAs innervating visceral organs, including the kidney and heart, remains unknown. The reason is that the human microneurographic technique is limited to measurements in the upper and lower extremities, face, and mouth.[2,5] Because the kidney and heart are important organs for circulatory control, the relation between muscle SNA and renal or cardiac SNA is very important. Accordingly, by recording calf muscle SNA by microneurography simultaneously with renal and cardiac SNAs in anesthetized rabbits, we sought to determine whether muscle SNA averaged over 1 minute truly parallels renal and cardiac SNAs in response to baroreflex forcing.

Methods

Animals were cared for in accordance with the Guiding Principles for the Care and Use of Animals in the Field of Physiological Science approved by the Japanese Physiological Society. Sixteen Japanese white rabbits (2.4 to 3.3 kg) were anesthetized by intravenous injection (2 mL/kg) of a mixture of urethane and α-chloralose[14] and were mechanically ventilated with O_2-enriched room air. Body temperature was maintained at 38°C with a heating pad. Arterial pressure (AP) was measured with a high-fidelity pressure transducer (Millar Instruments) inserted retrogradely from the right femoral artery.

After a retroperitoneal incision was made and a middle thoracotomy performed, left renal and left cardiac SNAs were recorded by stainless steel wire electrodes (Bioflex wire AS633, Cooner Wire).[14] After the flexors in the dorsal middle region of the right thigh were incised, a tungsten microelectrode (model 26-05-1, Federick Haer

Received July 20, 2004; revision received December 1, 2004; accepted December 27, 2004.

From the Department of Cardiovascular Dynamics (A.K., T.K., K.Y., D.M., H.A., T.M., K.U., M.S.), National Cardiovascular Center Research Institute, Osaka, and the Department of Cardiovascular Medicine (K.S.), Kyusyu University Graduate School of Medical Sciences, Fukuoka, Japan.

Correspondence to Atsunori Kamiya, MD, PhD, Department of Cardiovascular Dynamics, National Cardiovascular Center Research Institute, Osaka, 565-8565, Japan. E-mail kamiya@ri.ncvc.go.jp

Circulation is available at http://www.circulationaha.org

DOI: 10.1161/CIRCULATIONAHA.104.493338

Co) was inserted into the left tibial nerve to record muscle SNA, based on human[2,15] and animal[16] microneurography. We identified muscle SNA by the following discharge characteristics: (1) afferent activity induced by tapping of the calf muscles but not by gently touching the skin and (2) excitatory and inhibitory responses to a decrease and an increase in baroreceptor pressure, respectively. The nerve fibers peripheral to the electrodes were ligated securely to eliminate afferent signals. The preamplified signals of SNAs were bandpass filtered at 150 to 1000 Hz except those of muscle SNA in experiment 2 (480 to 5000 Hz). These signals were full-wave rectified and lowpass filtered (cutoff frequency, 30 Hz) to quantify nerve activity.

Experiment 1: Baroreflex Closed-Loop Condition

The rabbits were maintained in a supine position (n=6). All baroreceptor afferents and vagal nerves were intact. Three SNAs and AP were recorded at a 200-Hz sampling rate with a 12-bit analog-to-digital converter. After 2 minutes of baseline recording, nitroprusside (3 μg/kg) and, after a 2-minute delay, phenylephrine (3 μg/kg), was injected as a bolus via the right femoral vein. The data were stored on the hard disk of a dedicated laboratory computer system for later analysis.

Experiment 2: Baroreflex Open-Loop Condition

To strictly control baroreceptor pressure (n=10 rabbits), a baroreflex loop was opened by vascular isolation of the carotid sinuses.[14] Bilateral intracarotid sinus pressure (CSP) was controlled by a servo-controlled piston pump.[14] Bilateral vagal and aortic depressor nerves were sectioned at the middle of the neck to eliminate reflexes from the cardiopulmonary region and the aortic arch. After surgical preparation, CSP was increased stepwise from 40 to 160 mm Hg in increments of 20 mm Hg. Each pressure step was maintained for 60 seconds. The 3 SNAs were recorded and stored as in protocol 1.

Data and Statistical Analysis

We averaged SNAs over 1 minute and generated scatterplots for muscle SNA against renal or cardiac SNA. For each type of SNA, 100 and 0 arbitrary units (AU) were assigned to the maximum 1-minute SNA value and the noise level determined by intravenous infusion of hexamethonium bromide (6 mg/kg),[16] respectively. The other SNA signals were then normalized to these values. The correlation coefficients (r) for muscle SNA versus renal or cardiac SNA were determined.

In protocol 2, the relation between CSP and SNA was characterized by a 4-parameter logistic equation model: $y=P_4+(P_1/\{1+\exp[P_2(x-P_3)]\})$, where y is SNA and x is CSP; P_1 is the response range of SNA; P_2 is the coefficient for calculation of gain; P_3 is the CSP corresponding to the midpoint of the operation; and P_4 is minimum SNA. All data are presented as mean±SD, and $P<0.05$ was considered significant.

Results

In experiment 1 (baroreflex closed-loop condition), nitroprusside injection decreased AP by 16±3 mm Hg while muscle SNA was increased. Subsequent phenylephrine injection increased AP by 41±9 mm Hg while muscle SNA was decreased. Thereafter, as AP gradually decreased, muscle SNA was again increased. These responses of muscle SNA were similar to those of renal and cardiac SNAs (Figure 1A). When presented as SNA averaged over 1 minute, the relations of muscle SNA against renal SNA and cardiac SNA were both close to the line of identity (Figure 1B). All animals showed strong correlations between 1-minute muscle and renal SNAs (r=0.96±0.01, mean±SE; range, 0.93 to 0.98) and between 1-minute muscle and cardiac SNAs (r=0.96±0.01; range, 0.93 to 0.99).

In experiment 2 (baroreflex open-loop condition), muscle SNA decreased in response to nonpulsatile and stepwise

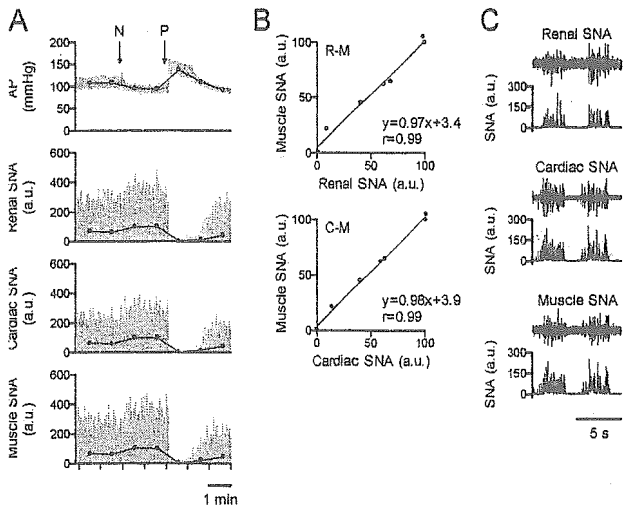

Figure 1. Experiment 1. A, Representative integrated signals of renal, cardiac, and muscle SNA during intravenous bolus injections of nitroprusside (time point N) followed by phenylephrine (time point P). Fine and bold lines indicate SNA signals resampled at 10 Hz and those averaged over 1 minute, respectively. B, Scatterplots of 1-minute muscle SNA against 1-minute renal and cardiac SNAs of same data shown in A. C, Representative original (upper panels) and integrated (lower panels) signals of 3 SNAs before pharmacological injection from 1 animal. R-M indicates renal vs muscle SNAs; C-M, cardiac vs muscle SNAs.

increases in CSP, similar to renal and cardiac SNAs (Figure 2A). All animals showed strong correlations between 1-minute muscle and renal SNAs (r=0.97±0.01; range, 0.96 to 0.99) and between 1-minute muscle and cardiac SNAs (r=0.97±0.01; range, 0.95 to 0.99). The baroreflex relation of muscle SNA against CSP was almost superimposable on that of renal or cardiac SNA in individual animals. The parameters in a reverse-sigmoid logistic function fitted in muscle SNA were similar to those in renal or cardiac SNA:

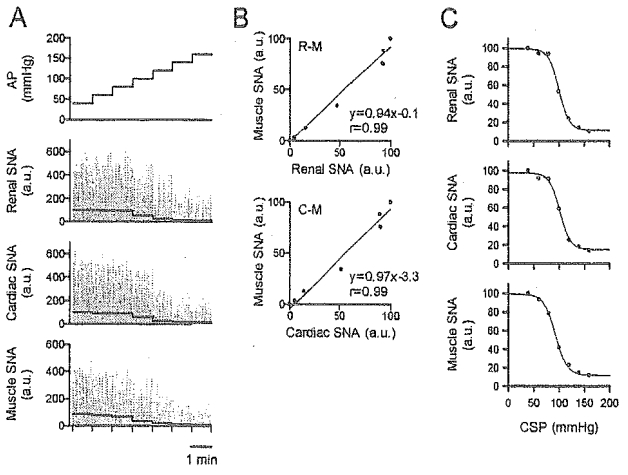

Figure 2. Experiment 2. A, Representative integrated signals of renal, cardiac, and muscle SNA during 1-minute stepwise increases in CSP from 1 animal. Fine and bold lines indicate SNAs resampled at 10 Hz and those averaged over 1 minute, respectively. B, Scatterplots of 1-minute muscle SNA against renal and cardiac SNAs. C, Sigmoidal baroreflex relation between each SNA and CSP. B and C used same data as shown in A. R-M indicates renal vs muscle SNAs; C-M, cardiac vs muscle SNAs.

P_1=99±1, 97±1, and 96±1 AU; P_2=0.11±0.02, 0.12±0.01, and 0.14±0.03 AU/mm Hg; P_3=99±4, 103±4, and 103±4 mm Hg; and P_4=3±2, 3±2, and 3±2 AU in muscle, renal, and cardiac SNAs, respectively.

Discussion

Despite accumulated data of muscle SNA as measured by microneurography in human studies, whether muscle SNA parallels other SNAs controlling cardiovascular organs remains unclear. The major new finding in this study is that 1-minute muscle SNA was correlated strongly with both renal and cardiac SNAs, with r at nearly unity, in both baroreflex closed- and open-loop conditions. This finding supports our hypothesis that muscle SNA averaged over 1 minute parallels renal and cardiac SNAs in response to baroreflex forcing. Our finding suggests that microneurographic muscle SNA is a useful proxy for renal and cardiac SNA in addressing baroreflex control of SNA.

Earlier human studies[3,4] reported that microneurographic muscle SNA was correlated with noradrenaline spillovers in the kidney (r^2=0.58) and heart (r^2=0.49) at rest, suggesting a correlation between muscle SNA and cardiac or renal SNA. However, because spillover values are affected by neurotransmitter kinetics in synapses (release and uptake) and circulating noradrenaline independent of SNA,[17] these results are not definitive. The present study complemented and extended the human studies by recording these SNAs directly and demonstrated stronger correlations (r>0.95) between muscle SNA and cardiac or renal SNA than earlier studies of spillover technique.

Previous studies reported a greater response of splenic SNA to baroceptor pressure changes than those of cardiac and renal SNAs in cats, suggesting regional differences in SNAs,[18] but those studies did not investigate muscle SNA. Additionally, these regional differences were detected in faster SNAs averaged over 4 to 8 seconds.[18,19] The present study investigated 1-minute SNA and hence did not address the relation between faster muscle SNA and renal or cardiac SNA.

The present study does not contradict earlier findings that indicated regionally different SNA responses to physiological stresses other than baroreceptor pressure changes. For example, the human cold pressor test increased muscle SNA but not heart rate.[20]

Limitations

The anesthetic, artificial respiration, and surgical procedures used in this study may affect SNAs. In addition, experiment 2 was performed under a nonphysiological condition and did not investigate baroreflex hysteresis. We bandpass filtered all SNAs at the same condition (150 to 1000 Hz) except muscle SNA in experiment 2 (480 to 5000 Hz, human study condition).[2] However, this did not affect the interpretation of data, because both experiments 1 and 2 showed strong correlations between muscle SNA and renal or cardiac SNA.

Conclusion

Muscle SNA averaged over 1 minute parallels renal and cardiac SNAs in response to a forced baroreceptor pressure change.

Acknowledgments

This study was supported by the Industrial Technology Research Grant Program, grant No. 03A47075, from the New Energy and Industrial Technology Development Organization of Japan.

References

1. Rowell LB. *Human Cardiovascular Control.* New York: Oxford University Press; 1993.
2. Mano T. Microneurography as a tool to investigate sympathetic nerve responses to environmental stress. *Aviakosm Ekolog Med.* 1997;31:8–14.
3. Wallin BG, Esler M, Dorward P, Eisenhofer G, Ferrier C, Westerman R, Jennings G. Simultaneous measurements of cardiac noradrenaline spillover and sympathetic outflow to skeletal muscle in humans. *J Physiol.* 1992;453:45–58.
4. Wallin BG, Thompson JM, Jennings GL, Esler MD. Renal noradrenaline spillover correlates with muscle sympathetic activity in humans. *J Physiol.* 1996;491:881–887.
5. Mitchell JH, Victor RG. Neural control of the cardiovascular system: insights from muscle sympathetic nerve recordings in humans. *Med Sci Sports Exerc.* 1996;28(suppl):S60–S69.
6. Victor RG, Pryor SL, Secher NH, Mitchell JH. Effects of partial neuromuscular blockade on sympathetic nerve responses to static exercise in humans. *Circ Res.* 1989;65:468–476.
7. Markel TA, Daley JC 3rd, Hogeman CS, Herr MD, Khan MH, Gray KS, Kunselman AR, Sinoway LI. Aging and the exercise pressor reflex in humans. *Circulation.* 2003;107:675–678.
8. Tanaka H, Davy KP, Seals DR. Cardiopulmonary baroreflex inhibition of sympathetic nerve activity is preserved with age in healthy humans. *J Physiol.* 1999;515:249–254.
9. Rudas L, Crossman AA, Morillo CA, Halliwill JR, Tahvanainen KU, Kuusela TA, Eckberg DL. Human sympathetic and vagal baroreflex responses to sequential nitroprusside and phenylephrine. *Am J Physiol.* 1999;276:H1691–H1698.
10. Grassi G, Cattaneo BM, Seravalle G, Lanfranchi A, Mancia G. Baroreflex control of sympathetic nerve activity in essential and secondary hypertension. *Hypertension.* 1998;31:68–72.
11. Grassi G, Seravalle G, Cattaneo BM, Lanfranchi A, Vailati S, Giannattasio C, Del Bo A, Sala C, Bolla GB, Pozzi M. Sympathetic activation and loss of reflex sympathetic control in mild congestive heart failure. *Circulation.* 1995;92:3206–3211.
12. Graham LN, Smith PA, Stoker JB, Mackintosh AF, Mary DA. Time course of sympathetic neural hyperactivity after uncomplicated acute myocardial infarction. *Circulation.* 2002;106:793–797.
13. Mosqueda-Garcia R, Furlan R, Tank J, Fernandez-Violante R. The elusive pathophysiology of neurally mediated syncope. *Circulation.* 2000;102:2898–2906.
14. Kawada T, Shishido T, Inagaki M, Tatewaki T, Zheng C, Yanagiya Y, Sugimachi M, Sunagawa K. Differential dynamic baroreflex regulation of cardiac and renal sympathetic nerve activities. *Am J Physiol Heart Circ Physiol.* 2001;280:H1581–H1590.
15. Sundlof G, Wallin BG. Human muscle nerve sympathetic activity at rest: relationship to blood pressure and age. *J Physiol.* 1978;274:621–637.
16. Nakamura T, Kawahara K, Kusunoki M, Feng Z. Microneurography in anesthetized rats for the measurement of sympathetic nerve activity in the sciatic nerve. *J Neurosci Methods.* 2003;131:35–39.
17. Jennings GL. Noradrenaline spillover and microneurography measurements in patients with primary hypertension. *J Hypertens Suppl.* 1998;16:S35–S38.
18. Ninomiya I, Matsukawa K, Honda T, Nishiura N, Nabuchi A, Nisimaru N, Irisawa H. Sympathetic nerve activity to the spleen, kidney, and heart in response to baroceptor input. *Am J Physiol* 1971;221:491–506.
19. Ninomiya I, Matsukawa K, Honda T, Nishiura N, Nabuchi A. Effects of baroceptor reflex on cardiac and renal sympathetic nerve activity before and after atropinization in awake cats at rest. *Jpn J Physiol.* 1988;38:491–506.
20. Fu Q, Levine BD, Pawelczyk JA, Ertl AC, Diedrich A, Cox JF, Zuckerman JH, Ray CA, Smith ML, Iwase S, Saito M, Sugiyama Y, Mano T, Zhang R, Iwasaki K, Lane LD, Buckey JC Jr, Cooke WH, Robertson RM, Baisch FJ, Blomqvist CG, Eckberg DL, Robertson D, Biaggioni I. Cardiovascular and sympathetic neural responses to handgrip and cold pressor stimuli in humans before, during and after spaceflight. *J Physiol.* 2002;544:653–664.

Am J Physiol Heart Circ Physiol 289: H1758–H1769, 2005.
First published June 2, 2005; doi:10.1152/ajpheart.01027.2004.

Low-frequency oscillation of sympathetic nerve activity decreases during development of tilt-induced syncope preceding sympathetic withdrawal and bradycardia

Atsunori Kamiya,[1,3] Junichiro Hayano,[2] Toru Kawada,[1] Daisaku Michikami,[1,3] Kenta Yamamoto,[1] Hideto Ariumi,[1] Syuji Shimizu,[1] Kazunori Uemura,[1] Tadayoshi Miyamoto,[1] Takeshi Aiba,[1] Kenji Sunagawa,[4] and Masaru Sugimachi[1]

[1]Department of Cardiovascular Dynamics, National Cardiovascular Center Research Institute, Osaka; [2]Core Laboratory, Nagoya City University Graduate School of Medical Sciences, and [3]Department of Autonomic Neuroscience, Research Institute of Environmental Medicine, Nagoya University, Nagoya; and [4]Department of Cardiovascular Medicine, Kyusyu University Graduate School of Medical Sciences, Fukuoka, Japan

Submitted 6 October 2004; accepted in final form 31 May 2005

Kamiya, Atsunori, Junichiro Hayano, Toru Kawada, Daisaku Michikami, Kenta Yamamoto, Hideto Ariumi, Syuji Shimizu, Kazunori Uemura, Tadayoshi Miyamoto, Takeshi Aiba, Kenji Sunagawa, and Masaru Sugimachi. Low-frequency oscillation of sympathetic nerve activity decreases during development of tilt-induced syncope preceding sympathetic withdrawal and bradycardia. *Am J Physiol Heart Circ Physiol* 289: H1758–H1769, 2005. First published June 2, 2005; doi:10.1152/ajpheart.01027.2004.—Sympathetic activation during orthostatic stress is accompanied by a marked increase in low-frequency (LF, ~0.1-Hz) oscillation of sympathetic nerve activity (SNA) when arterial pressure (AP) is well maintained. However, LF oscillation of SNA during development of orthostatic neurally mediated syncope remains unknown. Ten healthy subjects who developed head-up tilt (HUT)-induced syncope and 10 age-matched nonsyncopal controls were studied. Nonstationary time-dependent changes in calf muscle SNA (MSNA, microneurography), R-R interval, and AP (finger photoplethysmography) variability during a 15-min 60° HUT test were assessed using complex demodulation. In both groups, HUT during the first 5 min increased heart rate, magnitude of MSNA, LF and respiratory high-frequency (HF) amplitudes of MSNA variability, and LF and HF amplitudes of AP variability but decreased HF amplitude of R-R interval variability (index of cardiac vagal nerve activity). In the nonsyncopal group, these changes were sustained throughout HUT. In the syncopal group, systolic AP decreased from 100 to 60 s before onset of syncope; LF amplitude of MSNA variability decreased, whereas magnitude of MSNA and LF amplitude of AP variability remained elevated. From 60 s before onset of syncope, MSNA and heart rate decreased, index of cardiac vagal nerve activity increased, and AP further decreased to the level at syncope. LF oscillation of MSNA variability decreased during development of orthostatic neurally mediated syncope, preceding sympathetic withdrawal, bradycardia, and severe hypotension, to the level at syncope.

autonomic nervous system; baroreflex; blood pressure; heart rate variability; hemodynamics

HUMANS HAVE BEEN SUBJECTED to ceaseless orthostatic stresses since they first evolved and assume an orthostatic posture for most of their lives. During standing, gravitational fluid shift toward the lower part of body (i.e., abdominal vascular bed and lower limbs) would cause severe orthostatic hypotension if it were not countered by compensatory mechanisms (23). Orthostatic sympathetic activation has a crucial role in preventing orthostatic hypotension and maintaining arterial blood pressure (AP) (23). Recent studies have reported that orthostatic sympathetic activation is accompanied by an increase in low-frequency (LF, ~0.1-Hz) oscillation of sympathetic nerve activity (SNA) (1, 5). Tilt maneuvers of 75° and 80° greatly increase the LF oscillatory patterns of muscle SNA (MSNA), which mirrored similar changes in LF oscillation of AP (1, 5). However, LF oscillation of SNA has been investigated only in the steady-state orthostatic condition, when AP remains well maintained. It remains unclear whether LF oscillation of SNA changes during development of orthostatic neurally mediated syncope. Syncope is a common and potentially dangerous clinical syndrome (18). Under this condition, a major cause of hypotension is paradoxical withdrawal of sympathetic outflow to resistance vessels, because MSNA is greatly inhibited during hypotension (16–18), in addition to cardiac vagal excitation. Inasmuch as sympathetic activation is known to be accompanied by an increase in LF oscillation of SNA (1, 5, 15, 20, 24), it is possible that the increase in LF oscillation of SNA during orthostatic stress is not sustained during sympathetic withdrawal in the course of development of orthostatic neurally mediated syncope. Therefore, we hypothesized that LF oscillation of SNA decreases during development of orthostatic neurally mediated syncope. Because detailed characteristics, including LF oscillations of SNA during development of syncope, have not been studied in detail, we examine this phenomenon and attempt to explain the mechanism involved on the basis of current theories.

To test the hypothesis, we analyzed MSNA (by microneurography) and AP in 10 healthy male volunteers who manifested orthostatic neurally mediated syncope during the head-up tilt (HUT) test. Because sympathetic and cardiovascular changes during development of syncope are sudden and time dependent, traditional spectral methods, including autoregressive and fast Fourier transform power spectral analyses, cannot be used to assess these parameters. We therefore used the complex demodulation technique (8, 9, 13) to investigate dynamic changes in amplitudes of LF and respiratory high-

Address for reprint requests and other correspondence: A. Kamiya, Dept. of Cardiovascular Dynamics, National Cardiovascular Center Research Institute, 5-7-1 Hujishirodai, Suita, Osaka 565-8565, Japan (E-mail: kamiya@ri.ncvc.go.jp).

The costs of publication of this article were defrayed in part by the payment of page charges. The article must therefore be hereby marked "*advertisement*" in accordance with 18 U.S.C. Section 1734 solely to indicate this fact.

frequency (HF, ~0.25-Hz) oscillations of MSNA before and during tilt-induced orthostatic neurally mediated syncope.

METHODS

Subjects. Twenty healthy male volunteers [24 ± 4 (SE) yr old, 171 ± 5 cm, and 66 ± 5 kg body wt] underwent a passive 60° HUT test as described below. Ten of the subjects who developed orthostatic neurally mediated syncope or presyncope (syncopal group) were matched to 10 who remained asymptomatic during the procedure. Subjects with and without syncope were matched by age. The subjects were recruited from the local community through advertising on a notice board. They were carefully screened, with a medical history, physical examination, complete blood count, blood chemistry analyses, electrocardiogram, and psychological testing. Potential subjects with cardiovascular or other disease were excluded, as well as those who smoked tobacco products, drank alcohol, took medications other than oral contraceptives, or were obese (body mass index >30 kg/m^2). None of the subjects had experienced spontaneous syncope within the past 5 yr. All subjects had a sedentary lifestyle, and none were athletes. All subjects gave informed consent to participate in the study, which was approved by the Committee of Human Research of Research Institute of Environmental Medicine at Nagoya University.

Measurements. AP was measured continuously using a finger photoplethysmograph (Finapres, model 2300, Ohmeda, Englewood, CO). Systolic, diastolic, and pulse pressures were measured from the continuous pressure wave. Mean pressure was calculated by averaging pressure within a pulse wave. Finger pressure was confirmed to match intermittent (every minute) brachial AP measured by an automated sphygmomanometer (model BP203MII, Nippon Colin, Komaki, Japan). Electrocardiogram (chest lead II) and thermistor respirogram were also recorded continuously.

MSNA was measured as reported previously by our laboratory (14). Briefly, a tungsten microelectrode (model 26-05-1, Frederick Haer, Bowdoinham, ME) was inserted percutaneously into the muscle nerve fascicles of the tibial nerve at the right popliteal fossa without anesthesia. Nerve signals were fed into a preamplifier (Kohno Instruments, Nagoya, Japan) with two active band-pass filters set between 500 and 5,000 Hz and monitored with a loudspeaker. MSNA was identified according to the following discharge characteristics: *1*) pulse-synchronous and spontaneous efferent discharges, *2*) afferent activity evoked by tapping calf muscles, but not in response to a gentle skin touch, and *3*) enhancement during phase II of the Valsalva maneuver.

Protocols. Subjects were instructed to refrain from eating for 3 h before the experiments, which were conducted in an air-conditioned (26°C) room. Each subject was required to remain supine on a tilt bed set at 0° horizontally. After the microneurographic MSNA signal was detected, the subject remained at 0° supine and at rest for ≥20 min; then baseline MSNA, blood pressure, electrocardiogram, and respiration were recorded for 6 min. Thereafter, the tilt table was inclined to 60° in a passive manner and fixed for 15 min. The HUT was terminated and the table was returned to the 0° horizontal position when any of the following findings was observed: development of presyncope symptoms such as nausea, sweating, yawning, gray out, and dizziness and progressive reduction in systolic blood pressure to <80 mmHg. All variables were continuously monitored.

Data analysis. The full-wave-rectified MSNA signal was fed through a resistance-capacitance low-pass filter at a time constant of 0.1 s to obtain the mean voltage neurogram, which was resampled at 200 Hz, together with other cardiovascular variables. MSNA bursts were identified, and their areas were calculated using a custom-built (by our laboratory) computer program. MSNA was expressed as the rate of integrated activity per minute (burst rate) and total activity by integrating individual burst area per minute (total MSNA). Because burst area and, hence, total MSNA were dependent on electrode position, they were expressed as arbitrary units (AU) normalized by the individual baseline value at 0° supine rest (average of total MSNA per minute during 6 min of 0° supine rest was given an arbitrary value of 100 AU). The area of each burst during HUT was normalized to this value.

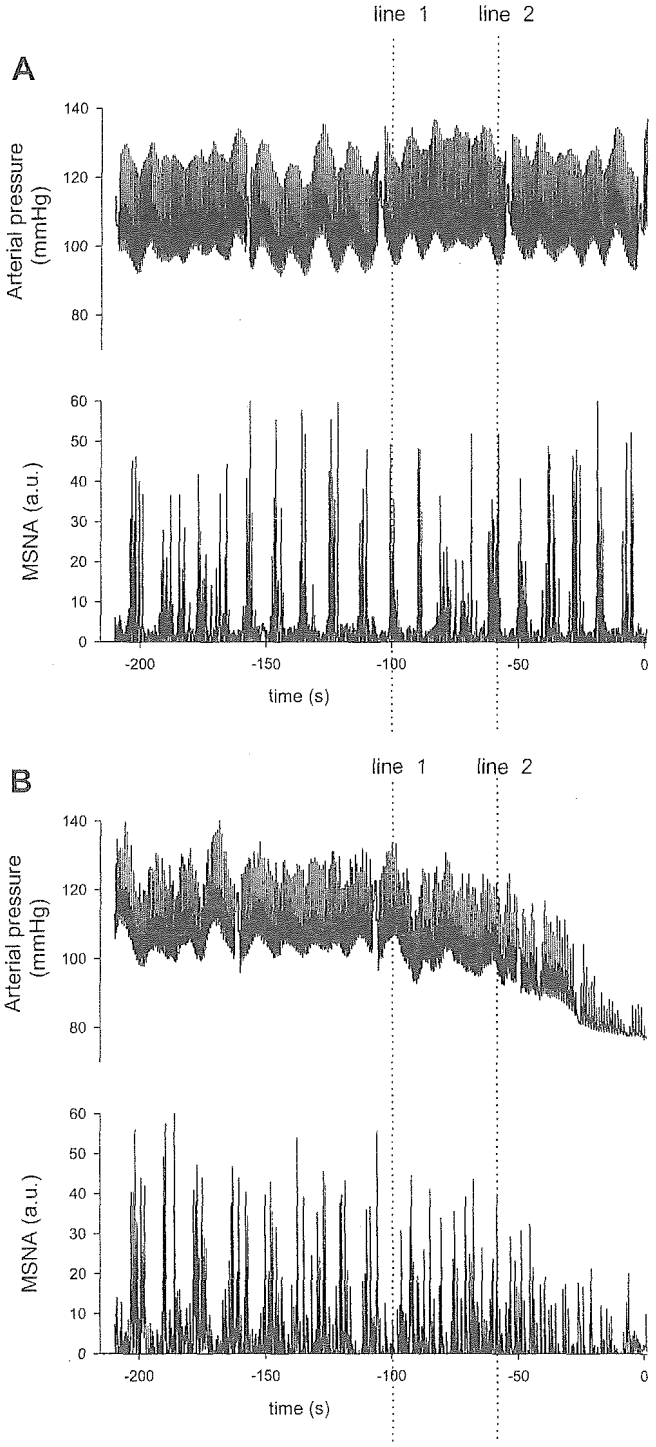

Fig. 1. Representative recordings of arterial pressure (AP) and muscle sympathetic nerve activity (MSNA, integrated signals) over 210 s before completion of head-up tilt (HUT) test in a nonsyncopal subject (*A*) and onset of syncope evoked by 60° HUT in a syncopal subject (*B*). *Time 0*, completion of HUT test (*A*) or onset of syncope when systolic AP decreases below 80 mmHg (*B*). *Line 1* and *line 2*, 100 and 60 s, respectively, before onset of syncope in HUT test.

Time-dependent changes in amplitudes of LF (0.04–0.15 Hz) and HF (0.15–0.35 Hz) components of MSNA, mean AP, and R-R interval variability were assessed continuously by complex demodulation using a custom-designed computer program (8, 9, 13). The complex demodulation technique is a nonlinear time-domain method of time series analysis suitable for investigation of nonstationary/unstable oscillations within an assigned frequency band (8, 9, 13). This method provides instantaneous amplitudes and frequency of LF and HF component variables as a function of time (8, 9, 13). For example, for a signal with 0.09- and 0.22-Hz oscillations at a given moment, this method calculates the instantaneous frequency of the LF and HF components as 0.09 and 0.22 Hz, respectively. In addition, the method provides the instantaneous amplitude of each oscillation. All neural and cardiovascular variables and their LF and HF components were averaged every 2 min during 0° supine rest and every 20 s during 60° HUT.

The squared coherence function was calculated as the square of the cross-spectrum normalized by the product of the spectra of the two different signals in the LF and HF bands (13). The periods analyzed were 0° supine (6 min), early HUT (first 5 min of HUT), from 100 to 60 s before onset of syncope, and from 60 s before to onset of syncope. The coherence function quantifies the amount of linear link between oscillations with the same frequency contained in two different signals. Coherence values >0.5 were considered significant.

Statistical analysis. Values are means ± SE. Repeated-measures analysis of variance was used to compare variables for time (every 2 min at 0° supine rest and every 20 s at HUT) and group (syncopal and nonsyncopal subjects). When the main effect or interaction term was significant, post hoc comparisons were made with Scheffé's F test. $P < 0.05$ was considered statistically significant.

RESULTS

All the syncopal subjects ($n = 10$) experienced neurally mediated syncope in the 60° HUT test. The end-of-HUT time was 10 ± 2 (range 7.8–13.8) min. All nonsyncopal subjects ($n = 10$) completed the 15-min 60° HUT test without a sign or symptom of neurally mediated syncope. Typical representative recordings of AP and MSNA in the nonsyncopal and syncopal subjects are shown in Fig. 1.

Nonsyncopal group. AP (systolic, diastolic, and mean) was maintained throughout HUT (Figs. 2 and 3). Pulse pressure decreased at the start of HUT and remained decreased below 0° supine levels throughout HUT ($P < 0.001$; Fig. 2). LF and HF amplitudes of mean AP increased at the start of HUT and remained above 0° supine levels throughout HUT ($P < 0.05$; Fig. 3). Magnitudes of MSNA (burst rate and total activity), as well as LF and HF amplitudes of MSNA variability, increased at the start of HUT and remained elevated above 0° supine levels throughout HUT ($P < 0.001$; Fig. 4). R-R interval and HF amplitude of R-R interval variability decreased below 0° supine levels throughout HUT ($P < 0.001$), whereas LF amplitude did not change (Fig. 5). Respiratory rate was nearly constant at 15 cycles/min. Instantaneous frequencies for LF and HF bands of all variables remained fixed at ~0.09 and 0.25 Hz, respectively (Figs. 2–5).

Syncopal group. Up to 100 s before the end of HUT, AP (systolic, diastolic, and mean) was well maintained (Figs. 2 and 3). MSNA, mean AP, pulse pressure, and R-R interval, as well

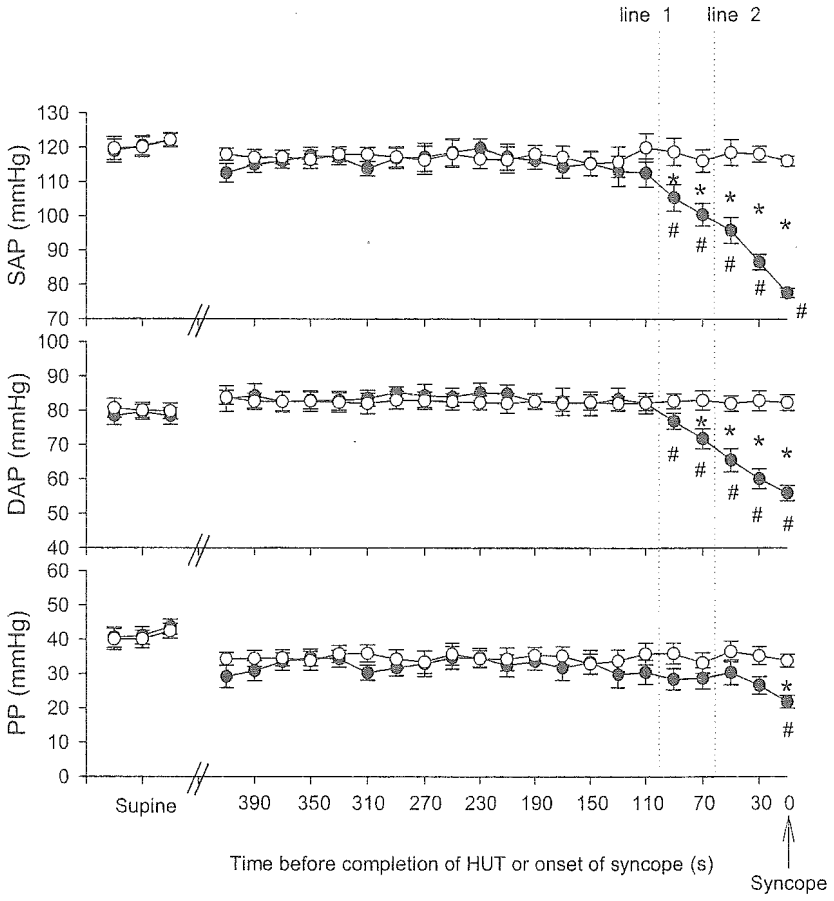

Fig. 2. Systolic AP (SAP), diastolic AP (DAP), and pulse pressure (PP) in syncopal (●) and nonsyncopal (○) subjects during 6 min of supine rest (averaged every 2 min) and during 410 s before completion of HUT test or onset of syncope in HUT posture (averaged every 20 s). *Line 1* and *line 2*, 100 and 60 s, respectively, before completion of HUT test or onset of syncope in HUT test. Pulse pressure in both groups is lower throughout HUT test than in supine posture ($P < 0.05$). *$P < 0.05$, syncopal vs. nonsyncopal. #$P < 0.05$ vs. mean for the first 100 s of HUT. Error bars, SE.